Upcycling waste into TiO_2 – Carbon dots-based and visible-light-active nano-photocatalysts

Diogo Gonçalo Martins Silva
Master in Environmental Sciences and Technology
Department of Geosciences, Environment and Spatial Plannings
Faculty of Sciences of the University of Porto
2025

Upcycling waste into TiO_2 – Carbon dots-based and visible-light-active nano-photocatalysts

Diogo Gonçalo Martins Silva

Dissertation carried out as part of the Master in Environmental Sciences and Technology

Department of Geosciences, Environment and Spatial Plannings

2025

Supervisor

Prof. Dr. Luís Pinto da Silva, Assistant Professor, Faculty of Sciences - University of Porto

CIQUP

IMS
Institute of Molecular Sciences

Acknowledgements

First and foremost, I would like to express my sincere gratitude to Professor Dr. Luís Pinto da Silva for accepting being my supervisor. I am also deeply thankful for all the patience he showed through this journey, for the guidance he provided, whether it was clarifying doubts or explaining the procedures of the work, and, above all, for always being present when I needed support the most. I am especially grateful for his encouragement to participate in IJUP2025, which proved to be an excellent opportunity to practice and improve my presentation skills.

I would also like to thank Professor Dr. Joaquim C. G. Esteves da Silva making available some the materials and resources necessary for its execution.

The research made during this dissertation was funded by the “Fundação para a Ciência e a Tecnologia, I.P.” (FCT, https://ror.org/00snfqn58), under the Grant 2023.13127.PEX.

In addition, I would like to acknowledge other individuals who made this experience much more enjoyable and facilitated my quick adaptation to laboratory work. The first of these is Ricardo Sendão, who played a fundamental role in the daily execution of this project His continuous support, dedication, and willingness to help were invaluable. He was always there, ensuring I never went home with unanswered questions.

I also received support from several others: Sónia Fernandes, a very cheerful and helpful person; Diana Crista, who was always in good spirits and, despite being pregnant and entitled to stay at home, chose to be with us every day, a testament to her remarkable character; Mr. Paulo, possibly the calmest person I have ever met, always with a smile on his face; Martinho and Mário, who are always in high spirits; and Yulia, a very kind person with whom one can have great conversations.

I would also like to thank Afonso Sousa, a classmate who has become a lifelong friend. He has been with me since my very first day at university, almost five years ago, which is quite something. I am grateful for all the conversations, lunches, and trips home together, especially since we became neighbors this year.

Finally, I would like to thank my family, especially my parents, my brother, and my dog, Rufus, for supporting me in every moment I needed them.

fct Fundação para a Ciência e a Tecnologia

Resumo

A crescente presença de corantes orgânicos em águas residuais leva à necessidade de procurar tecnologias eficientes e sustentáveis para a sua remoção, sendo uma das abordagens mais promissoras, o uso de nanopartículas (NPs) de TiO_2. No entanto, NPs de TiO_2 absorbem apenas de forma eficiente na região do ultravioleta (UV), o que motiva a exploração de novas abordagens que aumentem a sua eficiência sob luz visível, tais como a adição de *carbon dots* (CDs).

Assim, o objetivo principal deste trabalho é investigar como a modificação do TiO_2 com CDs derivados de biomassa influencia as suas propriedades físico-químicas e como essas alterações se traduzem diretamente no desempenho fotocatalítico sob luz visível.

Neste estudo, foram sintetizados CDs por via hidrotermal utilizando serrim. Estes CDs foram incorporados em NPs de TiO_2 para formar um NC ativo sob luz visível, o qual foi aplicado na degradação de corantes orgânicos, tais como Azul de Metileno (MB), Alaranjado de Metilo (MO), Rhodamina B (RhB), *Orange II* e *Remazol Brilliant Blue R* (RBBR). Testes com MB, mostraram um aumento de 675% na atividade fotocatalítica, resultado atribuído à melhor absorção na região visível e maior eficiência de utilização de fotões. Ensaios com *scavengers* de espécies reativas identificaram o radical anião superóxido ($\bullet O_2^-$) como o principal agente ativo na degradação. Avaliações complementares incluíram estudos de fotólise e medições do potencial de oxidação-redução (ORP), permitindo conhecer a capacidade *redox* do sistema.

Foi possível ver que apesar da adição de CDs levar genericamente a maior absorção de luz visível, maior capacidade de adsorção, e menor recombinação *electron-hole*, os NCs resultantes não têm necessariamente melhor atividade catalítica, podendo a atividade também ser determinada pelo tipo de espécies reativas de oxigénio (ROS) formada, e não só a sua quantidade.

Ao contrário de outros trabalhos que apenas relatam melhorias gerais, este estudo contribui para a compreensão dos mecanismos responsáveis por essa melhoria, estabelecendo uma ligação clara entre as propriedades fotoativas induzidas pelos CDs e o desempenho catalítico obtido. Estudos futuros deverão explorar a otimização da interação entre CDs e semicondutores, bem como avaliar a estabilidade e reutilização dos NCs em condições reais, reforçando o seu potencial para aplicações ambientais sustentáveis.

Palavras-chave: TiO_2, *carbon dots*, fotocatálise, corantes orgânicos, *scavengers*, serrim.

Abstract

The increasing presence of organic dyes in wastewater highlights the need for efficient and sustainable removal technologies, with TiO_2 nanoparticles (NPs) being one of the most promising approaches. However, TiO_2 NPs are only highly active under ultraviolet (UV) light, prompting the exploration of strategies to enhance their visible-light performance, such as the incorporation of carbon dots (CDs).

The main objective of this work is to investigate how the modification of TiO_2 with biomass-derived CDs affects its physicochemical properties and how these changes translate into photocatalytic performance under visible light.

In this study, CDs were synthesized via a hydrothermal route using sawdust. These CDs were incorporated into TiO_2 NPs to form a visible-light-active nanocomposite (NC), which was then applied in the degradation of organic dyes, including methylene blue (MB), methyl orange (MO), rhodamine B (RhB), Orange II, and Remazol Brilliant Blue R (RBBR).

Photocatalytic tests using MB showed a 675% increase in activity, attributed to enhanced visible-light absorption and more efficient photon utilization. Reactive species scavenger experiments identified the superoxide radical anion ($\bullet O_2^-$) as the primary active species involved in the degradation process. Additional evaluations included photolysis studies and oxidation-reduction potential (ORP) measurements to assess the redox capacity of the system.

Although the addition of CDs generally led to improved visible-light absorption, higher adsorption capacity, and reduced electron-hole recombination, not all resulting NCs exhibited enhanced catalytic activity. This indicates that the type of reactive oxygen species (ROS) generated, not merely their quantity, also plays a crucial role in determining photocatalytic performance.

Unlike previous studies that report only general improvements, this work provides deeper insight into the mechanisms responsible for enhanced activity, establishing a clear link between CD-induced photoactive properties and catalytic outcomes. Future studies should focus on optimizing the CD semiconductor interaction and assessing the stability and reusability of the NCs under real-world conditions, reinforcing their potential for sustainable environmental applications.

Keywords: TiO_2, carbon dots, photocatalysis, organic dyes, scavengers, sawdust.

Structure of the thesis

Chapter 1 (Introduction) highlights that the scarcity of potable water and the increasing contamination by organic pollutants demand effective and sustainable water treatment solutions. Heterogeneous photocatalysis using semiconductors, such as TiO_2, stands out as a promising technology. However, its application is limited by low visible-light absorption, rapid electron-hole recombination, and weak interaction with certain pollutants. In this context, CDs emerge as an efficient strategy to overcome these limitations. When conjugated with TiO_2, they may enhance visible-light absorption, facilitate charge separation by acting as an electron reservoir, and increase pollutant adsorption. Moreover, CDs can be synthesized from renewable organic residues, including biomass waste such as sawdust. Thus, this work aims to develop TiO_2-CD NCs to improve photocatalytic efficiency under visible light. The efficacy of these materials will be evaluated in the degradation of different textile dyes, comparing the results with the performance of TiO_2.

Chapter 2 (Materials and Methods) provides a detailed description of all experimental procedures used. It includes the hydrothermal synthesis and purification of CDs, the incorporation of CDs into TiO_2 to form NCs, and the various characterization techniques employed, such as BET, FTIR, SEM, UV-Vis and photoluminescence (PL) spectroscopy. The methodology of photocatalytic tests conducted with different dyes (MB, RhB, MO, Orange II, and RBBR), scavenger tests for reactive species identification, and ORP measurements are also explained.

Chapter 3 (Results and Discussion) presents experimental data and its critical analysis. The photocatalytic performance of the NC under visible light and its efficiency in degrading different dyes are discussed. The mechanisms of reactive species generation are analyzed, establishing correlations between the structural and optical properties of the materials and the observed catalytic outcomes. Redox potential is also examined to monitor reactive species generation during photocatalysis and to compare the behaviour of TiO_2 and the NC.

Finally, Chapter 4 (Conclusions and Future Works) summarizes the study's conclusions regarding the photocatalytic performance of the NCs in degrading some organic dyes, the underlying mechanisms, and the observed variations in efficiency with different dyes. It also discusses the limitations and key findings, followed by recommendations for future research aimed at optimizing the material, understanding the degradation processes, and evaluating practical applications under realistic conditions.

Table of Contents

List of Tables

List of Figures

List of Abbreviations and acronyms

AA	ASCORBIC ACID
AOPS	ADVANCED OXIDATION PROCESSES
BET	BRUNAUER-EMMETT-TELLER
BJH	BARRETT-JOYNER-HALENDA
CA	CITRIC ACID
CB	CONDUCTION BAND
CDS	CARBON DOTS
DRS	DIFFUSE REFLECTANCE SPECTROSCOPY
EDA	ETHYLENEDIAMINE
FTIR	FOURIER TRANSFORM INFRARED
IPA	SPECTROSCOPYISOPROPYL ALCOHOL
MB	METHYLENE BLUE
MO	METHYL ORANGE
MWCO	MOLECULAR WEIGHT CUT-OFF
NC	NANOCOMPOSITE
ORP	OXIDATION-REDUCTION POTENTIAL
PL	PHOTOLUMINESCENCE
RBBR	REMAZOL BRILLIANT BLUE R
RHB	RHODAMINE B
ROS	REACTIVE OXYGEN SPECIES
SA	SALICYLIC ACID
SEM	SCANNING ELECTRON MICROSCOPY
TTIP	TITANIUM (IV) ISOPROPOXIDE
UV	ULTRAVIOLET
VB	VALENCE BAND
VIS	VISIBLE

1. Introduction

1.1. Water availability, scarcity, contamination and current treatment techniques

Water is recognized as one of Earth's most vital resources, making its protection crucial to ensure a sustainable availability for future generations [1]. Although water is highly abundant on Earth, most of it consists of aquatic resources that are not directly accessible to humans, such as the saline waters of oceans and seas (97.2% of the total water mass) and glaciers (2.15%). Only approximately 0.65% of the planet's water consists of viable drinking water supplies [2]. Over time, it has become evident that, due to an increasing demand, the scarcity of freshwater is becoming an escalating threat to the sustainable development of human society [3]. Furthermore, rural-to-urban migration and population growth severely impacted water availability, leading to a rising demand and difficulties in wastewater management due to population sprawl. As traditional water sources become less viable, cities are turning to alternative sources like treated wastewater and stormwater runoff [4, 5]. At the same time, global climate change intensifies water scarcity, while also increasing the demand for energy, creating an imbalance that must be addressed. Ensuring access to safe water is not only critical for human survival, but also for the health and resilience of the surrounding ecosystems [6].

Aside from the rising water demand observed over the years, water pollution has also become a global issue in both developed and developing countries, requiring a continuous assessment of water resource policies in order to address this problem [7]. Currently, some technologies allow us to obtain freshwater from otherwise unsafe sources. These include seawater desalination, wastewater treatment and reuse and water condensation [8-10]. Seawater desalination is the process of removing salt from seawater to obtain fresh water, typically through reverse osmosis. Wastewater reuse involves treating used water to remove harmful substances, making it safe for reuse in applications such as agriculture, industry, or even as drinking water after advanced treatment. Finally, water condensation consists of the process of capturing water vapor from the air by cooling it, turning it into liquid water, thus producing drinking water from the atmosphere. However, seawater desalination and water condensation are costly and require a high amount of energy and thus are not economically viable [11-14].

Regarding contaminated wastewater, factors such as industrial effluents, urban runoff, direct waste disposal into water bodies, and agricultural fertilizers are some of the primary known water contaminants that leach into the environment [7]. Amongst the

diversity of pollutants found in wastewater, organic pollutants, such as pharmaceuticals, personal care products, pesticides and organic dyes, are increasingly recognized as being of particular importance [15, 16]. These substances often pose serious risks to both human health and ecosystems, and yet they are not typically monitored, increasing the risk of exposure. Furthermore, they are particularly difficult to remove due to their complex chemical structures and high persistence in water systems, leading to traditional wastewater treatment methods, such as conventional filtration and biological processes, being generally ineffective in their removal [17]. As a result, these pollutants often remain in treated effluents, entering natural water bodies and impacting aquatic life and human health [18]. Of particular concern is the treatment of wastewater effluents from the textile industry, which is estimated to be the largest industrial consumer of water globally and originates heavily contaminated wastewater, which is not efficiently treated and thus poses a risk to human health and the environment [19].

In fact, the toxicological phenomenon caused by organic pollutants is particularly harmful [20]. These compounds persist in the environment for exceptionally long periods due to their non-biodegradable nature, as they resist photolytic, chemical, and biological degradation [21, 22]. Additionally, they are of significant concern due to their long-range transport capability, persistence, and tendency to bioaccumulate. These compounds can bind to aerosols, allowing them to be transported from one location to another. As semi-volatile substances, they are capable of traveling long distances through the atmosphere, and within just a week, they can become globally distributed [23]. Once introduced into the food chain, they accumulate in human adipose tissue, posing a risk of adverse effects on both the environment and human health, so it becomes very crucial to remove these substances from the environment [24]. Some organic pollutants are deposited in marine and freshwater sediments, where both the sediment and the water act as long-term reservoirs. These reservoirs can reintroduce organic pollutants into the ecosystem and food chain over time [25, 26]. Exposure to these pollutants has been associated with a wide range of serious health issues, including endocrine disruption [27], various types of cancer [28], cardiovascular disease [29], obesity [30], reproductive and neurological disorders [31], and diabetes [32]. Moreover, prenatal exposure can lead to developmental defects in the embryo, particularly affecting fetal growth and organ formation in women during pregnancy [33].

Despite their highly persistent nature and tendency to bioaccumulate, we still use mostly conventional water treatment methods to try to remove these pollutants [34]. However, these methods may not achieve complete elimination of these highly complex toxic

organic compounds [35]. As mentioned before, many of these contaminants, such as pharmaceuticals, pesticides, and certain industrial chemicals, are resistant to biodegradation due to their low reactivity and high persistence in the environment. Additionally, traditional methods often lack the capacity to break down these pollutants into fully non-toxic forms and sometimes may even lead to degradation by-products that are more harmful than the initial pollutant [36]. As a result, these compounds may pass through treatment systems and continue to pose a risk to both human health and the ecosystem [37, 38].

As an alternative to traditional methods, advanced oxidation technologies (AOPs), such as photocatalysis, can also be used to treat wastewater. In fact, over the past decades, the treatment of aquatic pollutants through photocatalytic AOPs has been the focus of several studies [36, 39, 40]. Photocatalysis refers to promoting a reaction using irradiation as the energy source in a process mediated by a photocatalyst. It focuses on the conversion of light into chemical energy. The use of photocatalytic technologies has several advantages: it is a more environmentally friendly approach when compared to traditional chemical oxidation (i.e. less impactful than traditional methods), it achieves near complete degradation of the targeted pollutants, it may use an inexhaustible energy source (solar irradiation), and there are no by-products originating from the photocatalyst during the reaction [41-43].

1.2. Semiconductor photocatalysis

There are several studies concerning the photocatalytic treatment of wastewater with photocatalysts such as titanium dioxide (TiO_2) or zinc oxide [39, 44]. In these cases, the primary function of the catalyst is to catalyze the degradation of the contaminants; however, they can also be used toward the reduction of natural organic matter, disinfection, or serve as a pre-treatment step to enhance the efficiency of downstream treatment processes [2, 45, 46]. Currently, there is high interest in the use of photocatalytic technologies toward environmental remediation. This is understandable given that photocatalysis offers several advantages over conventional water treatment technologies, such as having a reduced equipment complexity, presenting non-selective oxidation capability, ease of operation, cost efficiency, and the possibility of achieving a virtually complete degradation of organic dyes into harmless byproducts [47].

Among all the available catalysts, semiconductors serve as a prime example of heterogeneous photocatalysts. Heterogeneous photocatalysis involves the interaction

between a light source and a solid semiconductor material suspended in a solution of a different physical state. In such systems, the reaction occurs at the surface of the solid catalyst upon light irradiation, leading to the degradation or transformation of pollutants. This phase separation allows for easy recovery and reuse of the catalyst, offering advantages such as improved stability, long-term durability, and cost-effectiveness [48]. Moreover, semiconductor photocatalysts possess a distinct energy band structure consisting of a lower-energy valence band (VB) and a higher-energy conduction band (CB), separated by an energy gap where no electronic states are available. This gap prevents the immediate recombination of photogenerated charge carriers, such as electrons and electron holes. This energy difference between the top of the filled VB and the bottom of the empty CB is referred to as the band gap [49].

Photocatalysis involves the activation of a semiconductor by light which, in the case of TiO_2, due to its large energy band gap, is typically ultraviolet (UV) light [50]. When TiO_2 absorbs suitable radiation, electrons in the VB are excited to the CB creating electron-hole pairs. The excited electrons in the CB can reduce oxygen molecules on the surface of TiO_2, forming superoxide radicals ($\bullet O_2^-$) while the holes in the VB can oxidize water or hydroxide ions (OH^-), generating hydroxyl radicals ($\bullet OH$) [51]. These reactive oxygen species (ROS) are highly reactive and interact with pollutants, breaking down their molecular structures. This leads to the degradation of organic contaminants into less toxic substances, eventually leading to a complete mineralization of the pollutant into CO_2 and water. This process is effective for environmental purification applications like wastewater treatment and air cleaning [52]. Figure 1 represents a typical mechanism for photocatalytic degradation, wherein the absorption of a photon with energy equal to or greater than the band gap excites the photocatalyst, originating photogenerated charge carriers that may originate reactive species such as $\bullet OH$ and $\bullet O_2^-$ [53, 54].

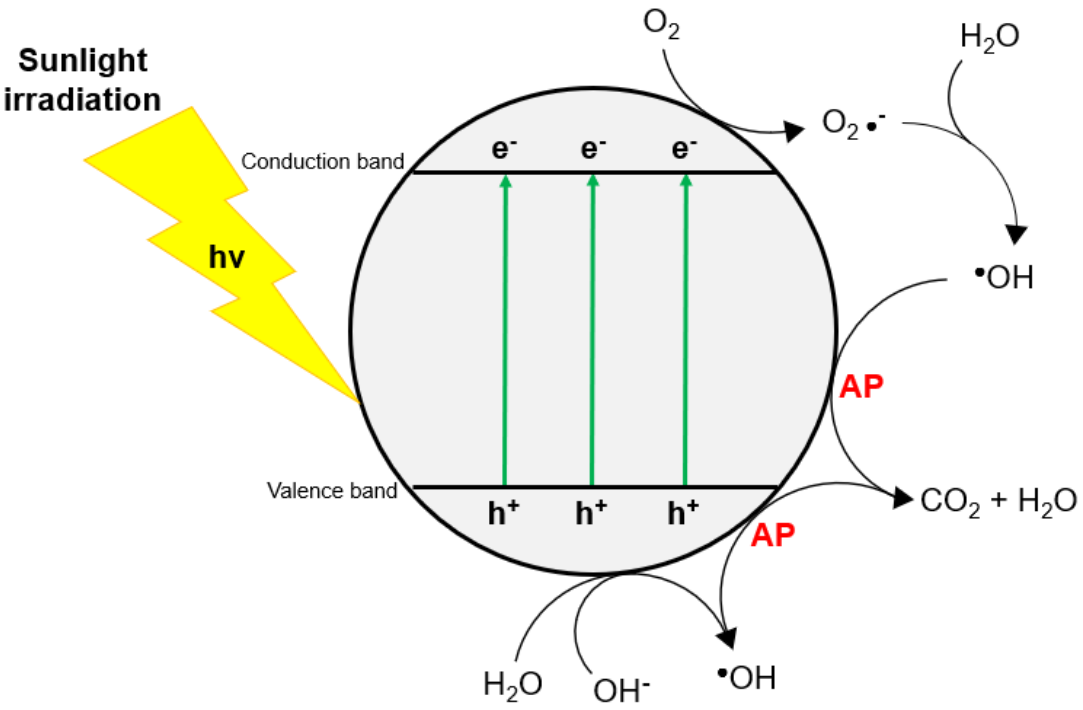

Figure 1: General photocatalytic reaction mechanism for a semiconductor. AP - adsorbed pollutant.

Perhaps the most widely used photocatalyst worldwide, TiO_2 is the natural oxide of titanium and a relatively inexpensive photocatalyst. It exhibits high activity under UV irradiation and has been proven effective toward the degradation of organic pollutants [44, 55, 56] and heavy metals [57]. Aside this, TiO_2 is also used for applications such as photocatalytic water splitting to generate hydrogen, a clean energy source and exhibits antibacterial and antiviral properties when exposed to UV light, making it useful in sterilization and medical applications [58, 59].

Commonly, TiO_2 is found in anatase and rutile forms, the two most common crystalline phases, which possess distinct band-gap energies that influence their photocatalytic efficiency, with anatase generally being the more active [60]. The use of nanostructured TiO_2 is advantageous for photocatalysis due to increased surface areas, low toxicity, biocompatibility, ease of nanostructure preparation, and faster reaction rates [61, 62]. Furthermore, TiO_2 surfaces can be readily modified, and their morphology can be tailored to include nanostructures [63], leading to enhanced mass transfer rates, improved adsorption of non-biodegradable organic compounds, and mesoporous surface properties [64]. TiO_2 nanoparticles (NPs) also exhibit a highly crystalline structure, an increased number of active sites and enhanced mass transfer rates [65]. This

characteristic makes TiO_2 a more energy-efficient and environmentally friendly alternative to conventional chemical oxidation processes [66].

Despite its advantages, TiO_2 also presents several drawbacks that hinder its commercial application. Its primary drawback is that its photocatalytic activity is mainly restricted to the UV region ($\lambda < 400$ nm), utilizing only about 5% of solar radiation [67]. This requirement for high-energy irradiation to overcome its bandgap (2.8–3.2 eV) severely limits its large scale application, as using TiO_2 solely with solar irradiation results in a low-efficiency process [68]. Additionally, TiO_2 suffers from rapid charge recombination, which reduces its photonic efficiency and leads to the loss of energy to non-productive processes that do not promote the catalytic reaction [69]. Furthermore, given that the semiconductor's surface has low affinity for organic pollutants and that photocatalytic degradation predominantly occurs on at a surface level, the degradation rate is limited as pollutants struggle to reach the active sites [70]. Finally, there is a certain tendency of TiO_2 NPs to agglomerate, which reduces their surface area and the availability of active sites, thereby decreasing photocatalytic efficiency [71].

It is no surprise that several strategies have been tested to bridge these limitations. Doping with metal and non-metal elements (e.g., platinum, nitrogen, and sulphur) may extend light absorption into the visible spectrum by introducing new energy levels [72]. However, doping can also accelerate charge recombination and raise concerns regarding cost and toxicity [73]. Regarding the surface's affinity toward organic pollutants, enhancements through co-catalytic systems and surface modifications have been explored to improve pollutant interaction, but those may also negatively impact the catalytic efficiency [74].

1.3. CDs: synthesis, properties and applications

Another alternative to bridge the limitations posed by using TiO_2 as a photocatalyst is to combine it with carbon nanomaterials such as carbon dots (CDs). Carbon is a black substance that, until recently, was believed to be insoluble in water and incapable of exhibiting fluorescence. While this holds true for its bulk form, carbon behaves quite differently at the nanoscale [75]. When carbon-based nanomaterials are synthesized, they reveal unique properties that are not present in the bulk material [76]. A variety of carbon nanomaterials have already been identified, including carbon nanotubes [77], carbon nanofibers [78], and, more recently, CDs [79-81]. Given that each type of carbon nanomaterial possesses distinct characteristics that not only differ from those of the bulk

material but also from one another, they offer tremendous potential for innovation in a wide range of applications.

CDs were first identified in 2004 by Xu et al. during the synthesis of carbon nanotubes [82]. The term “carbon dots” was later coined by Sun et al. in 2006 [83]. Since their initial discovery, CDs have attracted significant attention from the scientific community, largely due to their unique physicochemical properties and broad application potential [84]. One of their most notable features is a strong photoluminescence (PL) [85], which has sparked growing interest in their use as alternatives to conventional fluorescent materials. This interest has led to a rapid increase in research activity, with a marked rise in the number of publications focused on fluorescent NPs.

CDs are typically sized between 1 and 10 nm, although larger sizes may be occasionally observed [86]. They normally exhibit a spherical or quasi-spherical morphology, with the core potentially being either amorphous or nanocrystalline, depending on the source of the NPs [87]. On the surface, functional groups such as amines, alcohols, or carboxylic acids are commonly present, which significantly contribute to the excellent water solubility of CDs [86]. These surface groups also enable further chemical modifications, allowing for passivation and functionalization [88]. Such modifications provide a chemical platform for coupling additional molecules, which can enhance the photoluminescent properties of the CDs or modify their physical characteristics and interactions with other molecules [86, 88, 89]. The properties of CDs are highly tuneable and are influenced by several factors, including the composition of the precursors, reaction conditions, the synthetic methodology used, and any post-synthesis treatments applied [90]. As a result, the internal and external structure and composition of the NP can vary significantly [85].

The synthesis of CDs can be achieved through either top-down or bottom-up approaches (Figure 2) [91]. Top-down methods involve the fragmentation of carbon-based materials at the macro or microscale using techniques such as laser ablation [92], arc discharge [93], and chemical oxidation [94]. Laser ablation employs high-energy laser pulses directed at carbon targets immersed in solvents, promoting the formation of CDs with good crystallinity [92]. Arc discharge entails the sublimation of carbon electrodes under electrical current [93], while chemical oxidation utilizes strong acids, such as nitric and sulfuric acid, to degrade graphitic structures and release functionalized CDs, although it requires rigorous purification steps [94]. Despite yielding well-structured materials, these methods present limitations regarding selectivity, the use of toxic reagents, and the need for specialized equipment.

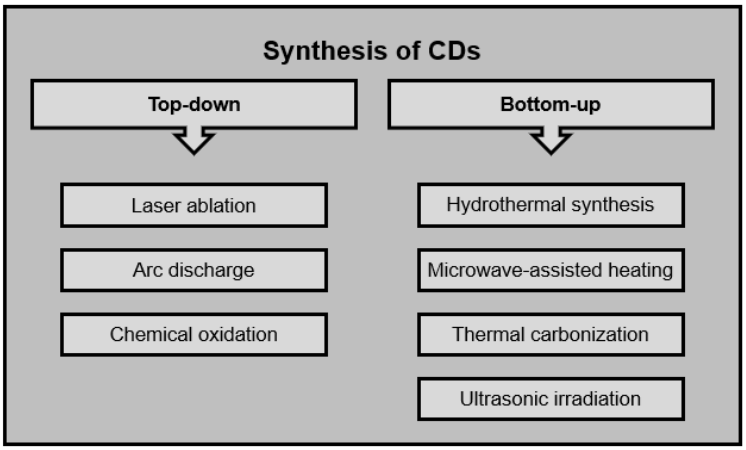

Figure 2: Synthesis of CDs through top-down or bottom-up approaches.

In contrast, bottom-up methods are simpler, more sustainable, and offer greater control, relying on the carbonization of small organic molecular precursors through routes such as hydrothermal synthesis [95], microwave-assisted heating [96], thermal carbonization [97], and ultrasonic irradiation [98]. Hydrothermal synthesis, one of the most widely employed techniques, involves the reaction of precursors like citric acid (CA) or urea in aqueous solvents under high temperature and pressure in sealed autoclaves, enabling the formation of CDs with high dispersion and surface functionalization [95]. Microwave-assisted synthesis enables the rapid conversion of precursors into CDs within minutes [96], while thermal carbonization involves heating organic compounds such as biomass or sugars at moderate temperatures, making it an environmentally friendly and economically viable approach [97]. Ultrasonic treatment is also explored to induce chemical reactions and the nucleation of CDs, providing good control over particle morphology [98].

The choice of synthesis method depends on the desired properties of the final material, including particle size and distribution, fluorescence intensity and stability, degree of surface functionalization, as well as economic feasibility, scalability, and environmental impact of the process [99].

Bottom-up approaches are generally preferred over top-down methods due to their simplicity, lower cost, shorter reaction times, and minimal equipment requirements [100]. Among these, microwave irradiation and hydrothermal treatment are the most widely employed, often using nitrogen-containing dopants to enhance optical properties [101, 102]. These methods offer tuneable emission characteristics and, when natural precursors are used, typically allow for one-step syntheses without the need for post-synthetic surface passivation, as surface oxidation occurs during the process [103].

Moreover, by selecting appropriate precursors and reaction conditions, it is possible to obtain hydrothermally synthesized CDs capable of emitting across the entire visible spectrum [104, 105]. These advantages make microwave irradiation and hydrothermal treatment particularly attractive methods for the efficient fabrication of CDs with tailored optical properties, while reducing time and resource consumption.

Among its properties, CDs exhibit a high PL [87, 106, 107], broad optical absorption range [108], biocompatibility [83, 86, 109], low toxicity [110], high photostability and chemical stability [88, 111], excellent water solubility [87, 88] and a high degree of tunability in terms of their physical and optoelectronic properties [112, 113]. As a result of these unique characteristics, CDs have a wide range of practical applications, including bioimaging [114], sensing and biosensing [115-117], drug delivery systems [118], photodynamic therapy [119], light-emitting devices [120], nanothermometry [121], photovoltaic devices [122], and photocatalysis [123, 124], with notable examples involving TiO_2/CDs nanocomposites (NCs) [125, 126].

1.4. Use of CDs to bridge TiO_2's limitations

Due to their characteristics, CDs may offer a potential solution to overcome the limitations of TiO_2, thereby potentially improving its photocatalytic performance. The core of CDs primarily consists of sp^2-hybridized carbon atoms interconnected by sp^3 carbon atoms, and their surface can be functionalized with various chemical groups [86, 88]. This unique structure is believed to grant them a high electron storage capacity, potentially allowing photoexcited electrons from the CB of TiO_2 to be transferred to the carbon nanostructure (Figure 3). As a result, the photocatalytic process may be extended into the visible region and the charge carrier separation may become more efficient, which can lead to an enhanced photonic efficiency [127]. This may be due to the transfer of e^- from the CB of TiO_2 to the CDs, promoting a better separation of the photogenerated charge carriers, thus enhancing the overall photocatalytic efficiency. Additionally, the functionalized surface of CDs may enhance the photocatalyst's ability to adsorb pollutants, potentially increasing the quantity of contaminants that reach the active site for degradation [128]. The possibility of an improved visible-light activation, enhanced charge separation via electron transfer between CDs and TiO_2, and improved pollutant adsorption, may collectively contribute towards an improved photocatalytic performance.

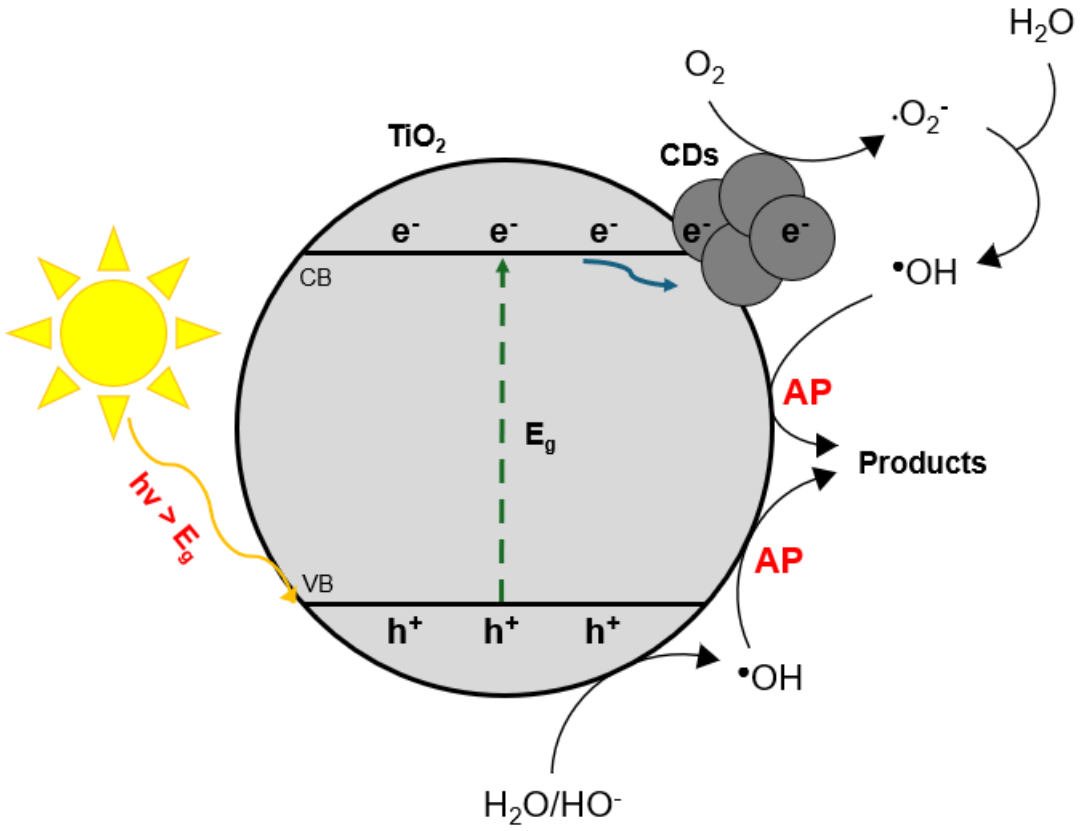

Figure 3: Representation of the possible degradation mechanism of TiO_2 - CDs NCs.

1.5. Biomass-derived CDs and circular economy

In addition to potentially improving TiO_2's photocatalytic efficiency, another advantage of CDs is the fact that they can be prepared from a range of precursors that includes organic waste/biomass, which can be used as a viable alternative to commercially available chemical reagents that are more harmful towards the environment [129, 130]. In fact, the conversion of biomass into carbon materials is regarded as part of the shift from a linear economy into a circular economy.

In a linear economy, the traditional process consists of three steps: extraction, manufacture and disposal [131]. Companies design products, purchase raw materials, transform the raw materials into final products, and sell them. The products are used until the end of their life cycle and are discarded, generating large amounts of waste. To reduce the impact of waste, a solution is needed that allows for the continuous reuse of resources.

This leads to the transition to a circular economy, which promotes waste reduction and resource efficiency, thereby improving sustainability and economic potential in a zero-waste system. As a prime example, biomass sources are considered a better option compared to fossil fuels due to their abundance, low cost, and sustainability, resulting in a circular economy and lower environmental impacts as we are using a waste that would otherwise be discarded. In summary, having solutions that promote a circular economy and facilitate the energy transition contributes to climate change mitigation and reduces our dependence on non-renewable resources [132].

Examples of renewable precursor sources used for the preparation of CDs include plant-based/agricultural waste, such as sawdust from wood production [133], corn husk [134], and other types of waste, such as food scraps and peels [135, 136]; marine waste, such as glycogen obtained from mussel cooking wastewater [137], chitin extracted from crustacean shells (e.g., shrimp, squid) [138], and chondroitin sulphate/gelatine from the cartilage and skin of blue sharks [139]; by-products of industrial processes, such as coconut shells [140]; and finally, innovative sources, including microalgae/aquatic biomass [141] and coffee grounds [142, 143]. A specifically important example for our work is the application of carbon materials made from wood sawdust [133], which can be used in the production of photocatalytic NCs for wastewater treatment under visible-light irradiation, which is ultimately the focus of our study.

The use of sawdust, an abundant waste in the wood industry, as a carbon source provides environmental benefits, as it reduces the use of commercial reagents and the associated environmental impacts [144]. In fact, CDs derived from sawdust have gained attention due to their eco-friendly and sustainable production methods [145]. For example, they have been used in applications such as bioimaging [146], sensing [147], and photocatalysis for the degradation of organic pollutants [44, 148, 149]. These sawdust-derived CDs have also shown promise in drug delivery systems and light-emitting devices due to their excellent photoluminescent properties.

1.6. Objectives

Given the limitations of TiO_2, which is primarily activated by UV light and thus ineffective under solar irradiation, there is a growing interest in modifying this material to enhance its visible-light photocatalytic activity. One promising strategy is the incorporation of CDs, which have shown potential in improving the visible-light responsiveness and charge separation of the resulting NCs. However, many of existing studies concerning this kind

of material only explore the photocatalytic improvement for a single model pollutant, leaving unclear whether these improvements extend across different pollutants [150, 151]. Moreover, most of the reported CDs are based on synthetic precursors, overlooking the opportunity to valorize waste materials. In this context, the use of biomass waste, such as sawdust, a byproduct of the wood industry, as a carbon source for CDs, introduces a more sustainable and circular approach to the preparation of these NPs.

For this study, organic dyes were chosen as target pollutants due to the environmental concerns associated with dye-containing effluents and their persistence in aquatic systems. Namely, the objectives of this work were to develop visible-light-active NCs by incorporating CDs derived from sawdust into TiO_2 and evaluate their respective photocatalytic performance in the degradation of several representative textile dyes. A comparative approach was adopted using TiO_2 as a reference, aiming to assess whether the addition of CDs effectively improves photocatalytic activity and if these enhancements are consistent across different types of dyes.

From this work resulted one communication at a national scientific conference.

Communication:

- Diogo Silva, Ricardo Sendão, Luís Pinto da Silva, Study of waste-based carbon dots for application in TiO_2-based photocatalytic nanocomposites, 18º Encontro de Investigação Jovem da Universidade do Porto, 2025, Porto (Portugal) – oral communication.

2. Materials and Methods

2.1. Materials

Titanium (IV) isopropoxide (TTIP, 99.99 %), CA (99.5 %), ethylenediamine (EDA, 99 %), Rhodamine B (RhB, 95 %), Orange II (85 %), Remazol Brilliant Blue R (RBBR), Salicylic acid (SA) (≥99.0%), Ascorbic Acid (AA) (≥99.7%), Tiron (4,5-Dihydroxy-1,3-benzenedisulfonic acid disodium salt monohydrate) and TiO_2 NPs (99.7 %, <25 nm particle size, anatase phase) were acquired from Sigma Aldrich. Isopropyl alcohol (IPA, 99.9 %) was bought from Fisher Chemical. Methylene Blue (MB) was obtained from Carlo Erba. Methyl Orange (MO) was obtained from Honeywell Fluka. All commercially acquired reagents were utilized as they were received.

The sawdust was supplied by a Portuguese company. Before using the material, the sawdust was dried for 24 hours at 105 ºC in a VWR DL 112 Prime oven (2500W). The sawdust was then stored in a freezer at -80 ºC to prevent the growth of microorganisms.

2.2. CDs synthesis and purification

The synthesis procedure employed in this study follows previously reported methods, utilizing CDs that have been characterized in a previous work [145]. The CDs were synthesized via a hydrothermal method using CA and sawdust as co-carbon sources and EDA as an N-dopant, as represented in Figure 4. Initially, 0.075 g of sawdust and 0.075 g of CA were added to a Teflon-lined vessel. Subsequently, 10 mL of 0.01 M sodium hydroxide (NaOH) solution and 166.9 µL of EDA were also added. The mixture was then subjected to ultrasonic treatment for 30–60 seconds to enhance the dispersion of the components. Following this, the Teflon vessel was sealed inside a stainless-steel reactor and heated in an oven (VWR DL 112 Prime, 2500 W) at 200 °C for 8 hours. After the hydrothermal treatment, the reaction product was allowed to cool down to room temperature. It was then subjected to ultrasonic treatment for 20 minutes to promote the solubilization of the CDs. The resulting solution was transferred to a Falcon tube and diluted with deionized water to a final volume of 10 mL. The sample was centrifuged for 30 minutes to remove any large particulates. Afterwards, the supernatant was then placed into a dialysis membrane with a molecular weight cut-off (MWCO) of 3500 Da. Dialysis was carried out for 24 hours to remove residual impurities that could alter the CDs' properties and reactivity [111]. The sample was then lyophilized for 48 hours. The resulting dry solid was weighed, resuspended in deionized water, and the final

concentration of CDs calculated. The particles were kept in the cold (4 ºC) until further use.

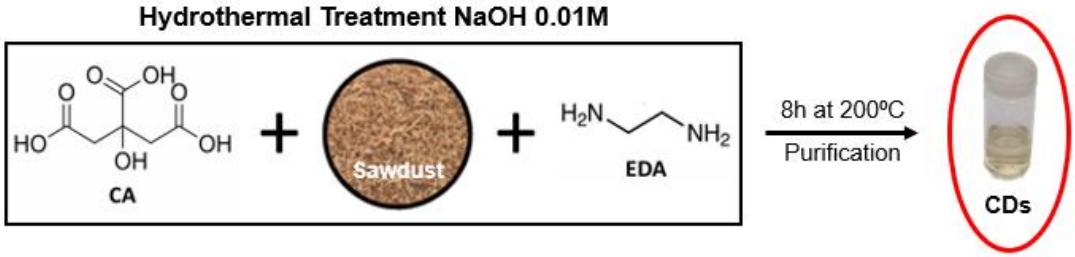

Figure 4: Schematic representation of the synthesis and purification of the CDs employed in the photocatalytic NC.

2.3. TiO_2/CDs Nanocomposite Preparation

This study is focused on investigating the degradation mechanisms of different dyes using a NC. The synthesis of the NC was described based on an adapted methodology previously employed by our research team [148], as illustrated in Figure 5.

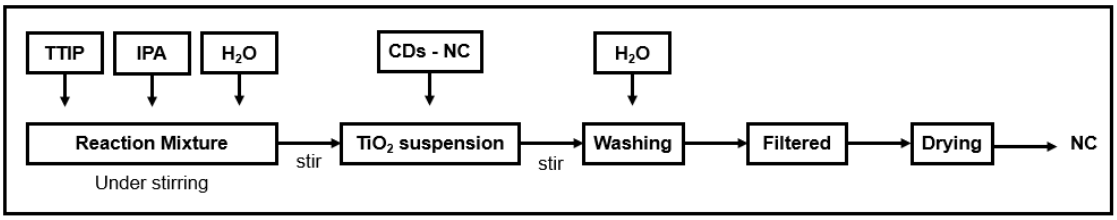

Figure 5: Representation of the steps employed to prepare the NC. TTIP - titanium isopropoxide; IPA - isopropyl alcohol; H_2O - deionized water; CDs - NC - CDs prepared previously to be incorporated in the NC; NC - nanocomposite.

Briefly, NC was prepared via a sol-gel methodology [148, 152]. For an expected yield of 0.1 g of NC, 2.395 mL of IPA and 0.371 mL of TTIP were added dropwise into a beaker under continuous stirring. The mixture was stirred for 30 minutes to ensure complete dispersion of the titanium precursor. Subsequently, 2.25 mL of deionized water were added to the beaker, and the solution was stirred for an additional 2 hours. Upon the addition of water, a white coloration developed due to the hydrolysis of TTIP, which led to the formation and precipitation of TiO_2 NPs at the bottom of the beaker. In parallel, a second solution was prepared by adding 5 mL of deionized water and an appropriate volume of CDs (corresponding to 4% of the target NC mass) under stirring. The mixture was maintained at 70 °C for 2 hours prior to being added dropwise to the TiO_2 NPs. The

combined mixture was then stirred for an additional 2 hours and subsequently filtered. The solid retained on the filter paper was transferred to a watch glass and dried overnight in an oven at 100 °C. The dried material was then gently ground using a mortar and pestle into a fine powder and placed in a muffle furnace at 300 °C for 3 hours (Thermolyne 47900 muffle, 1000 W). After cooling, the final TiO_2/CD NC was collected for further use.

2.4. Materials Characterization

The photocatalysts' absorption profiles in powder form were recorded using UV-Vis diffuse reflectance spectroscopy (DRS). The equipment used for this was a Jasco V-760 spectrophotometer with an integration sphere (Jasco ILV-924) addon. Barium sulphate was used as the reference.

PL spectra were collected via a Horiba Jovin Yvon Fluoromax-4 spectrofluorometer in standard 10 nm fluorescence quartz cells. The experiments were conducted using water-based dispersions of the materials at different concentrations. For MB, a concentration of 2.5 mg/L was used, with an excitation wavelength of 665 nm. For the other dyes, the following conditions were applied: 5.0 mg/L and 465 nm excitation for MO, 2.5 mg/L and 550 nm RhB, 6.5 mg/L and 485 nm for Orange II, and 55.5 mg/L and 592 nm for RBBR. The data was processed and analysed via the FluorEssence software provided with the equipment.

The morphology of TiO_2 and NC was obtained via high-resolution scanning electron microscopy (SEM), in CEMUP – Materials Centre of the University of Porto. Namely, a FEI Quanta 400 ESEM FEG system was used to analyse powder samples scattered in a carbon tape. Average sizes for the catalysts were obtained by calculating the average size of 100 individually measured particles.

Infrared spectra were collected using a Vertex70 (Bruker) FT-IT spectrophotometer coupled to a Specac Golden Gate Single Reflection Diamond Attenuated Total Reflectance addon. The spectra were analyzed in the range of 4000–500 cm^{-1} with a spectral resolution of 4 cm^{-1}. The analysis was carried out at FCUP|DQB – Lab&Services, Department of Chemistry and Biochemistry, Faculty of Sciences, University of Porto.

The surface area and pore parameters were determined using a nitrogen adsorption analyzer (TriStar Plus, Micromeritics, Norcross, GA, USA). Prior to conducting the N_2

adsorption-desorption measurements, the samples were degassed under N2 flow at 200°C for 6 hours to remove adsorbed water and volatile impurities, ensuring that the measured surface area and pore characteristics reflect only the properties of the materials and not those of surface contaminants. The pore size distributions were calculated using the desorption branch of the N_2 isotherms, applying the Barrett-Joyner-Halenda (BJH) method. The analyses were performed at the RT4 group of CIQUP by Dra. Ana Brandão, under the supervision of Prof. Carlos Pereira.

2.5. Photocatalytic activity assays

The visible-light catalytic potential of TiO_2 and NC was evaluated under visible-light irradiation using a MainHouse energy-saving lamp (23 W, 6400 K, 1311 Lm) as irradiation source, which had already been used by our team in previous works [153, 154].

In a normal experimental setup, 0.020 g of the NC was added to 100 mL of a 2.5 mg L^{-1} solution of MB. Subsequently, a 2 mL sample is collected 30 minutes prior to irradiation (used to assess the adsorption of the pollutant by the catalysts when compared to t_0). The reaction mixture is then stirred in the dark for 30 minutes to establish an adsorption-desorption equilibrium, collecting the second sample, t_0. Afterwards, the irradiation source is switched on and four more samples are collected at consecutive 15-minute intervals of irradiation at t_{15}, t_{30}, t_{45}, and t_{60}. The collected aliquots are then centrifuged at 10000 rpm for 30 minutes to separate the heterogeneous catalyst from the pollutant prior to spectrophotometric analysis, via a Horiba Jovin Yvon Fluoromax-4 spectrofluorometer in standard 10 nm fluorescence quartz cells.

The absorbance readings of each sample are then recorded at the specific maximum absorption wavelength for each dye, i.e. 665 nm (MB absorption peak, εm = 73460 M^{-1} cm^{-1}) for MB [155]. These tests, like shown in Figure 6, were also performed with other dyes, namely RhB at 550 nm, MO at 465 nm, Orange II at 485 nm and RBBR at 592 nm, in addition to MB. Their respective concentrations were adjusted so that A = 0.5 at their absorption peaks.

To determine the apparent reaction rate constant, the natural logarithm of C/C_0 is plotted as a function of time, and the slope of the resulting linear fit corresponds to the reaction rate constant.

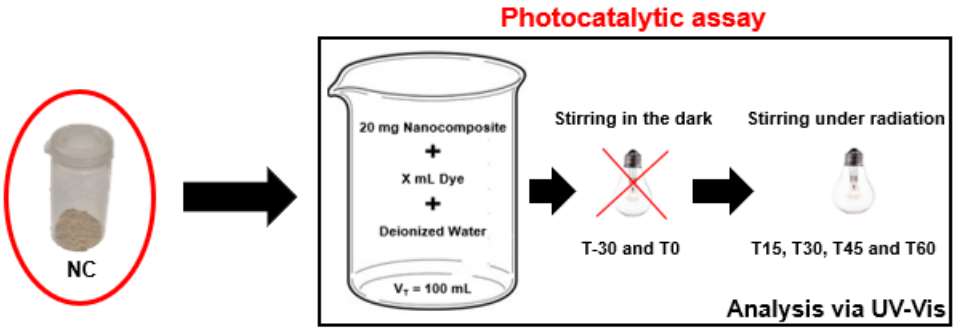

Figure 6: Schematic representation of the catalytic assays performed with the NC.

2.6. Free Radical Scavenger Test

To evaluate the role of each reactive species during the photodegradation of MB, scavenger tests were conducted using specific scavengers for different free radical species. The impact of these scavengers on the catalytic system was monitored to assess their influence. ●OH and $●O_2^-$ were selectively inhibited using IPA (10 mM) [154] and Tiron (10 mM) [156], respectively. Additional tests were performed employing SA (10 mM) and AA (10 mM) as semi-quantitative approaches for measuring and evaluate the production of ●OH and $●O_2^-$, respectively. For these tests, all reaction conditions were as described in the "Photocatalytic activity tests" (60 min of irradiation). Finally, the pollutant removal rates obtained in the presence of each scavenger were compared to those from control experiments conducted without any scavenging agents.

2.7. ORP

To evaluate the tendency of a substance to gain or lose electrons in an oxidation-reduction reaction, ORP tests were conducted. This test indicates the ability of a solution to oxidize (remove electrons from a substance) or reduce (add electrons to a substance). For the experiments, 10 mg of TiO_2 or NC were added to 50 mL of deionized water in a 100 mL beaker. The suspension was kept in the dark for 30 minutes, followed by 60 minutes of visible-light irradiation, employing the same irradiation source used in the previous experiments, under constant stirring, with the ORP electrode (HI4430B by Hanna Instruments) continuously in contact with the solution, using a Conductivity Bench Meter (HI5521 by Hanna Instruments). During the experiment, measurements were recorded whenever the ORP values varied by at least 1%. At the end, the ORP values obtained with TiO_2 and NC were compared. It is known that positive ORP values are indicative of oxidizing capacity, whereas negative ORP values reflect reducing capacity.

However, changes in ORP values after a stimulus, such as an increase or decrease, can suggest a shift in the redox state of the system. ORP values are measured in millivolts (mV) and are crucial in various chemical processes, such as water treatment.

3. Results and discussion

3.1. Characterization

To better understand the properties of the NCs and to evaluate in which ways they could affect the photocatalytic activity in comparison to TiO_2, we started by characterizing the morphology, structure, and optical properties of the catalysts via UV-Vis / PL spectroscopy, SEM, BET and FTIR. TiO_2 and TiO_2-CDs NCs were compared in terms of optical properties.

First, the UV-vis spectra were obtained. Analysis of their optical absorption spectra (Figure 7a) revealed that, although both materials exhibit strong absorption in the UV region, the incorporation of CDs into the NC significantly enhanced its absorption in the visible range (400 to 700 nm). This indicates that the NC possesses a markedly greater capacity for visible-light absorption compared to TiO_2, whose absorption beyond 400 nm is minimal. Several factors may account for the observed enhancement in light absorption. Literature suggests that Ti^{3+} ions can form as a result of electron transfer interactions between TiO_2 and the CDs, which contributes to increased absorption at wavelengths above 600 nm [157]. Therefore, the still significant absorption beyond 600 nm in the NC is likely indicative of residual Ti^{3+} species. The improved absorption in the 400–600 nm range, on the other hand, could be attributed to the CDs themselves, which are known for their broad spectral absorption and thus may enhance the overall light-harvesting ability of the composite. This hypothesis may not carry much weight on its own, as the article that first described these CDs showed that their absorbance is, after all, only significant in the UV region [145]. Consequently, the incorporation of CDs into TiO_2 enhances its visible-light absorption either directly, through their intrinsic optical properties, or indirectly, by promoting the formation of Ti^{3+}.

To further evaluate the optical properties, DRS data were used to estimate the band gap energies of TiO_2 and the NC using Tauc's plot ($(\alpha h\nu)^2 = h\nu$), where α represents the absorption coefficient and hv is the photon energy. The calculated band gap values were 3.27 eV for TiO_2 and 3.17 eV for the NC. These results suggest that although visible-light absorption was significantly improved, the reduction in band gap energy was relatively modest.

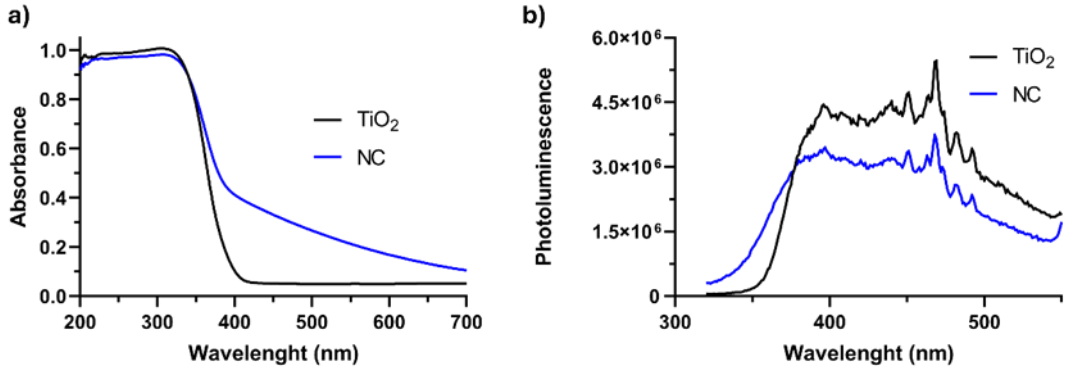

Figure 7: a) UV-Vis DRS spectra of TiO_2 and the NC and b) steady-state PL spectra of TiO_2 and NC.

The PL spectra of both catalysts were analysed to investigate the influence of CDs on the suppression of photogenerated charge carrier recombination. This is based on the fact that PL may result from the recombination of the photogenerated charge carriers and therefore a decrease in PL intensity may indicate a lower degree of charge recombination. As shown in Figure 7b, both the NC and TiO_2 exhibit a broad emission band spanning from 350 to 600 nm. However, the incorporation of CDs into TiO_2 led to a marked reduction in the PL intensity. According to previous studies, this decrease suggests that the interaction between the semiconductor and the carbon material facilitates rapid electron transfer across the interface formed between them [148, 158]. Moreover, due to their distinctive structural features, the CDs act as electron reservoir, effectively trapping photogenerated charge carriers and thereby inhibiting the recombination of electrons and holes in TiO_2 [159]. Consequently, less energy is lost through radiative recombination, as reflected by the diminished PL intensity, meaning that more energy is still available to drive the catalytic reactions, thus promoting the catalytic efficiency.

The morphology of TiO_2 and the NC were analysed via SEM (Figure 8). Similar to other TiO_2-based photocatalysts, the NC presents a round shape with an average size of 72.2 ± 12.5 nm [160, 161]. On the other hand, TiO_2 presented an average size of 24.7 ± 4.2 nm, which is well in line with what we expected given the nature of the NPs we used (purchased from Sigma-Aldrich, size ≤25 nm. Furthermore, the NC seems to have a larger tendency towards forming aggregates, which can be ascribed to the CDs' functionalized surface. Several functional groups such as carboxyl, carbonyl and amine groups are commonly found on the surface of these nanomaterials and are prone to originate electrostatic interactions and form hydrogen bonds between themselves, promoting the agglomeration of the NC particles [162].

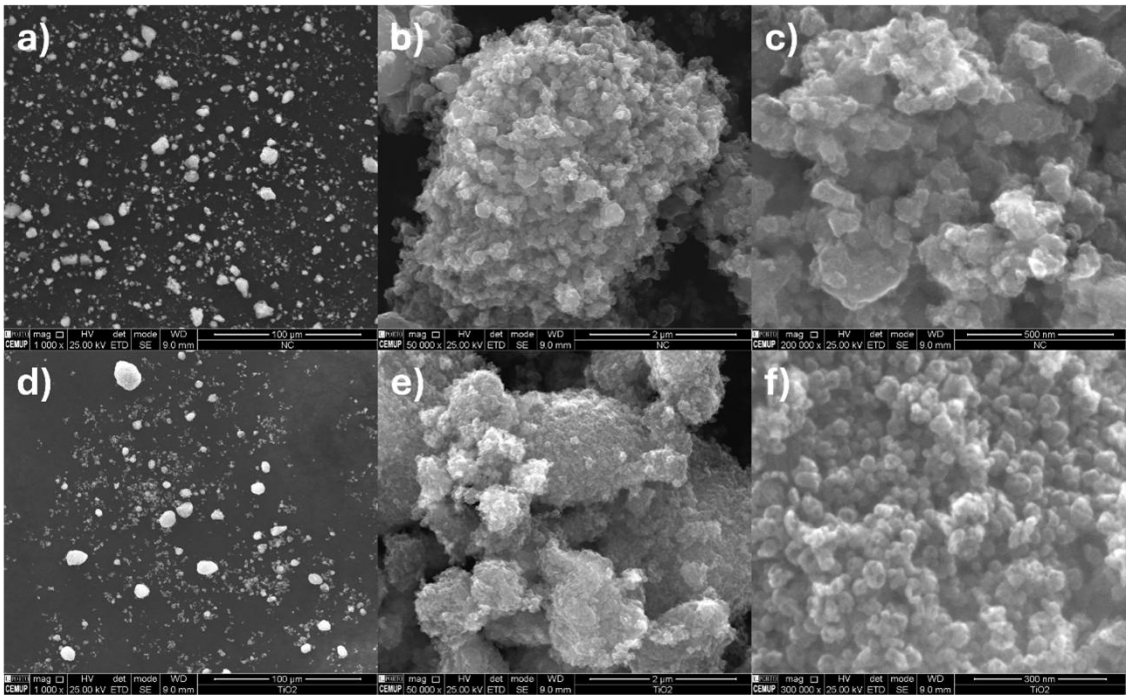

Figure 8: SEM images of the NC at a) 1000x, b) 50 000x and c) 100 000x magnification; TiO_2 at d) 1000x, e) 50 000x and f) 100 000x magnification.

Table 1: Surface area, pore volume and pore size for TiO_2 and NC.

Sample	S_{BET} ($m^2\ g^{-1}$)	V_{total} ($cm^3\ g^{-1}$)	D_p (nm)
TiO_2	105.2	0.276	13.1
NC	154.8	0.157	4.0

Data resulting from Brunauer-Emmett-Teller (BET) analysis revealed that the NC presents a higher specific area (S_{BET}) than TiO_2 (Table 1). Namely, the results suggest that both TiO_2 and NC have similarities with Type III isotherms (Figure 9a), the NC presents a S_{BET} of 154.8 $m^2\ g^{-1}$, ca. 1.5x higher than that presented by TiO_2 (105.2 $m^2\ g^{-1}$). This increased surface area means that there is more space to adsorb the pollutant. Regarding pore size, both TiO_2 and NC are classified as mesoporous, presenting pore widths of 13.1 and 4.0 nm, respectively (estimated via the Barrett-Joyner-Halenda (BJH) method with pore size distribution represented on Figure 9b [163].

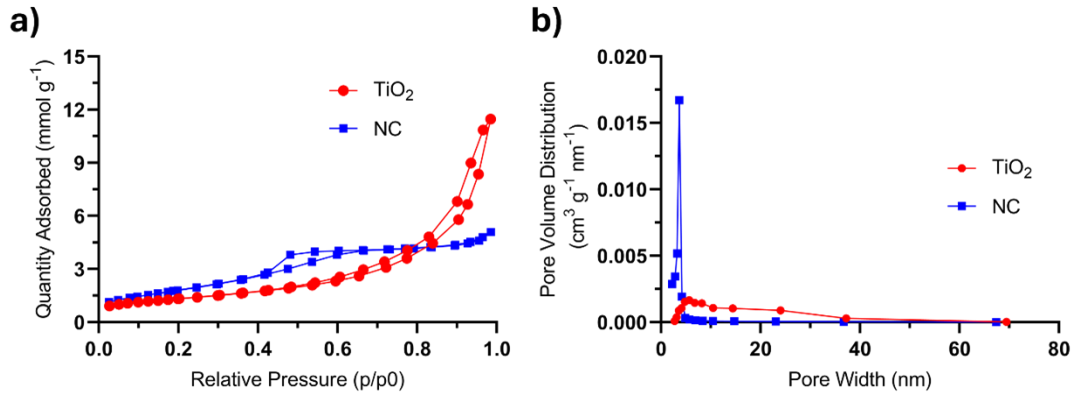

Figure 9: a) N_2 adsorption-desorption isotherms and b) pore volume distribution calculated by the BJH pore size distribution method for TiO_2 and NC.

The Fourier Transform Infrared Spectroscopy (FTIR) spectra were also obtained for TiO_2 and NC (Figure 10). Both catalysts presented a similar profile with a small peak at ca. 1630 cm^{-1} being attributed to carbonyl groups and H-O-H stretching vibrations [164], a wide band centred at ~3200 cm^{-1} ascribed to the stretching vibration of -OH groups of either adsorbed water or carboxylic acids from the CDs [165] and a peak arising at wavelengths under 800 cm^{-1} that is attributed to the vibration of Ti-O-Ti bonds, which is expected given the anatase structure associated with TiO_2 and our NC [165]. The similarity between the two materials suggests that the addition of CDs did not prompt any major changes in the composition of the resulting photocatalyst.

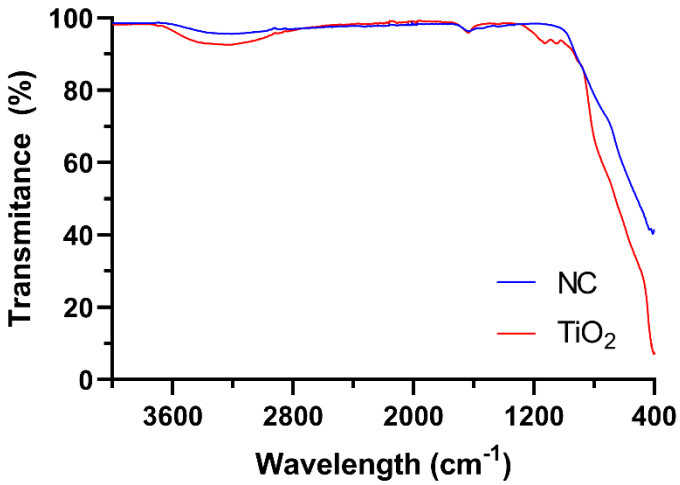

Figure 10: FTIR spectra of TiO_2 and the NC.

3.2. Photodegradation of Different Dyes

For the NC, as mentioned before, CDs were produced via hydrothermal treatment (200 ºC for 8 h) using sawdust and CA as carbon precursors. The CDs were mixed (4 wt%) into TiO_2 prepared from TTIP, obtaining the NC. The characterization of the materials suggests that adding CDs to TiO_2 significantly increased the visible-light absorption and photonic efficiency activity under visible-light irradiation, as well as the surface area of the material. Overall, these results would be expected to provide the NC with superior photocatalytic activity compared to TiO_2. Given these improvements, further tests with a model organic pollutant should demonstrate an enhanced photocatalytic efficiency under visible-light irradiation.

The visible-light-driven photodegradation potential of the NCs was analysed by measuring the visible-light-driven photocatalytic degradation of the dyes via UV-Vis spectrophotometry. To compare these results to those of TiO_2, we quantified the amount of pollutant removed over a set irradiation time (%DR, Eq. 1) [166] and calculated the associated rate constant (Eq. 2). To calculate the %DR, we employed the following equation:

$$\%DR = \frac{C_0 - C_t}{C_0} \times 100 \quad (1)$$

Here, %DR corresponds to the % of textile dye removed over a set time of irradiation, C_0 represents the initial concentration of the dye in the mixture, and C_t is the concentration of the dye after an irradiation period of *t* minutes. Furthermore, the kinetics and reaction rate constant of the degradation follows a pseudo-first-order reaction that can be written as follows [167]:

$$-\ln\left(\frac{C_t}{C_0}\right) = kt \quad (2)$$

In Eq. 2, C_t corresponds to the concentration of the dye after an irradiation period of *t* minutes, C_0 corresponds to the initial dye concentration, *k* is the estimated rate constant, and *t* is the time of sample irradiation with a visible-light source. In either case, the dye concentration was obtained via analysis of the absorbance at 550 nm for RhB [168], 465 nm for MO [169], 665 nm for MB [155], 485 nm for Orange II [170] and 592 nm for RBBR [171], via UV-Vis spectrophotometry.

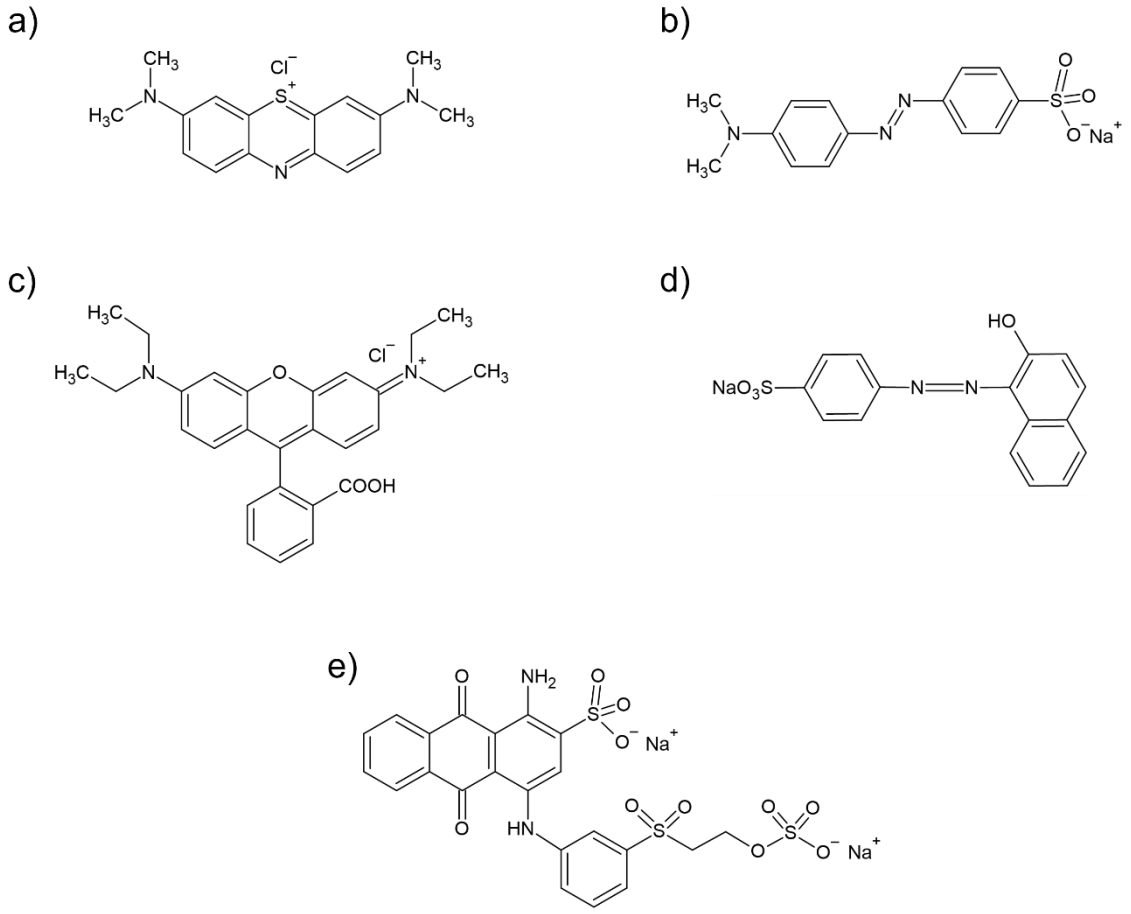

Figure 11: Molecular structure of each dye: a) MB, b) MO, c) RhB, d) Orange II and e) RBBR.

To assess the photocatalytic potential of the NC, we compared the photodegradation efficiency of different dyes by TiO_2 and the NC. Namely, experiments were conducted using MB, MO, RhB, Orange II and RBBR as target pollutants, as these dyes are commonly employed in the literature as model organic contaminants for evaluating photocatalytic activity due to their well-characterized structures (Figure 11), distinct optical properties, and environmental relevance [152, 172, 173]. In these experiments, the required dye concentrations were calculated to achieve an initial absorbance of approximately 0.5. The irradiation time was set to one hour instead of extending it to achieve complete degradation, because the focus of this study is primarily qualitative and comparative. Our main goal is to compare the performance of the catalysts relative to TiO_2 rather than obtaining absolute degradation values. Conducting the experiments with a fixed one-hour irradiation allows us to observe clear differences in %DR and k between the photocatalysts. Although longer irradiation times would lead to higher overall pollutant degradation, the %DR values reported here do not represent the maximum degradation achievable by the photocatalysts.

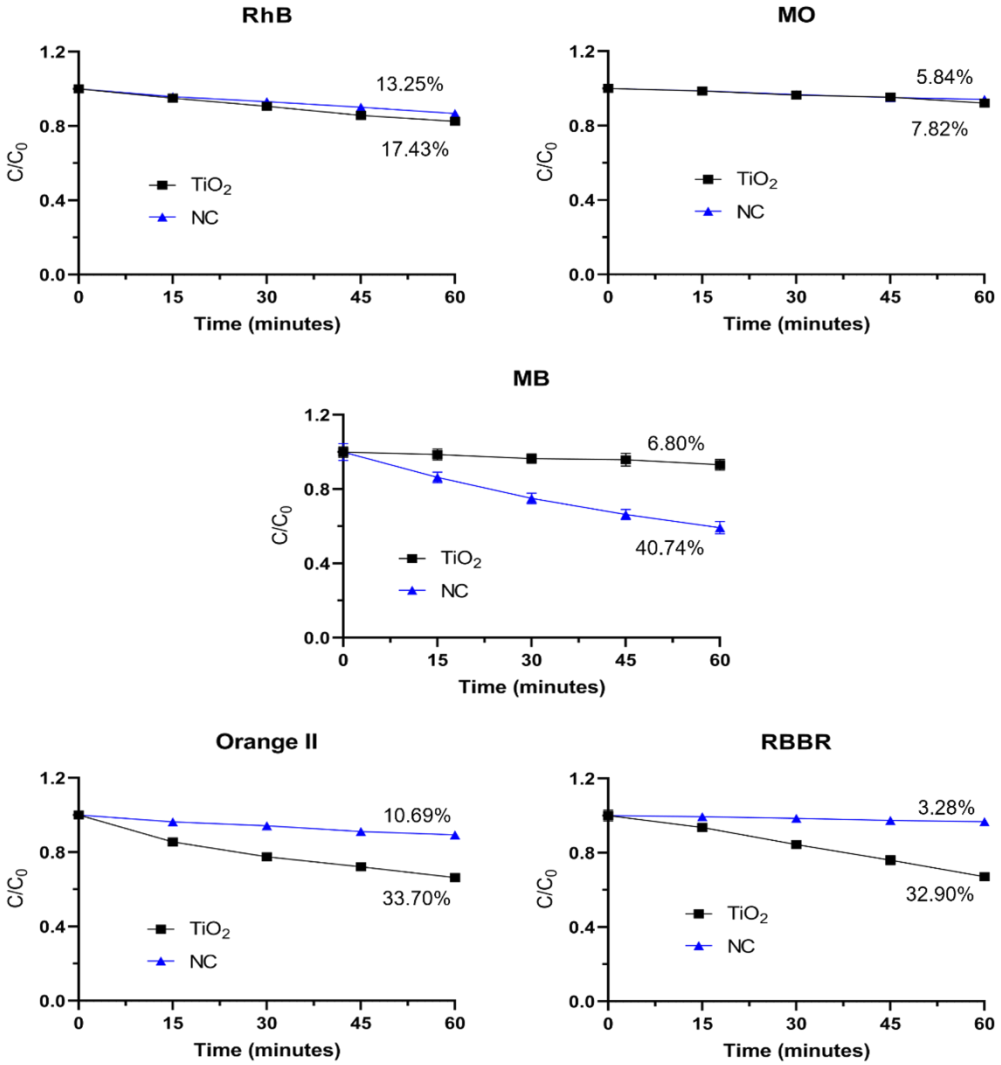

Figure 12: Photodegradation of different dyes catalysed by TiO_2 and NC under visible-light irradiation. The percentage values presented in the graph correspond to the %DR of each dye.

As shown in Figure 12, the NC exhibits distinct photodegradation behaviours depending on the dye tested. For MB, the NC demonstrated significantly better performance compared to TiO_2, with %DR of 40.74% and 6.80% (with degradation rate constant of 0.0087 min^{-1} and 0.0011 min^{-1} respectively). In this case, the addition of CDs significantly enhanced the photocatalytic efficiency when compared with TiO_2. However, for RhB and MO, no significant changes in the photodegradation were observed, with the performance of NC and TiO_2 being similar. For RhB and MO, TiO_2 showed %DR values of 17.43% and 7.82% (with degradation rate constants of 0.0032 min^{-1} and 0.0013 min^{-1}, respectively), while the NC achieved 13.25% and 5.84% (with degradation rate constants of 0.0023 min-1 and 0.0010 min-1, respectively), respectively. On the opposite end, adding CDs to TiO_2 toward the photodegradation of Orange II and RBBR resulted

in a decrease in catalytic efficiency when compared to TiO_2, with the CDs thus having a completely opposite effect on the catalytic efficiency when compared with the photodegradation of MB. In the case of Orange II and RBBR, the degradation efficiencies for TiO_2 were 33.70% and 32.90% (with degradation rate constant of 0.0066 min^{-1} and 0.0067 min^{-1} respectively), whereas the NC reached only 10.69% and 3.28% (with degradation rate constant of 0.0019 min^{-1} and 0.00058 min^{-1} respectively), showing a substantial decline. The %DR and reaction rate constant values for each dye, both with NC and TiO_2, can be seen in Table 3.

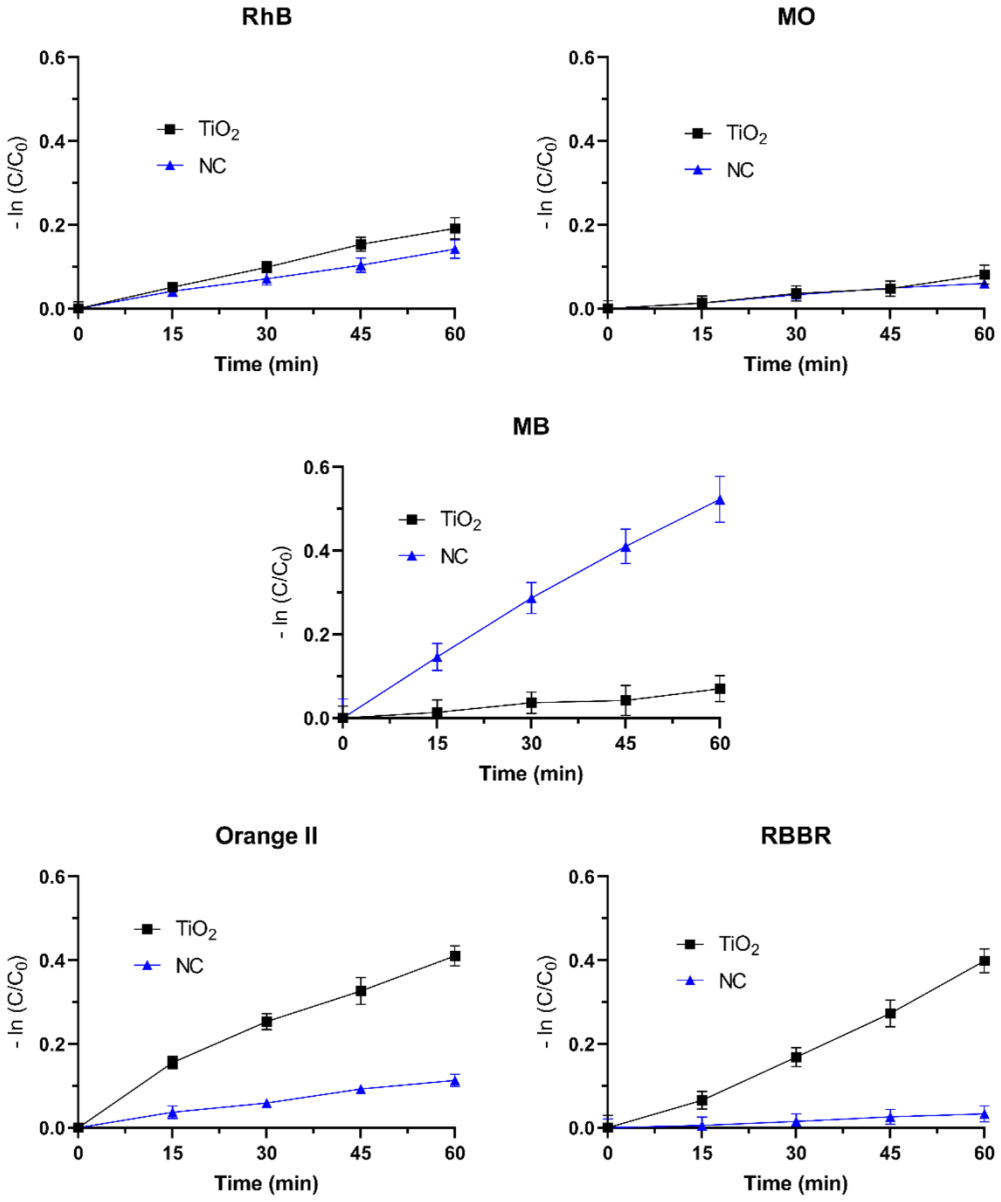

Figure 13: Representation of -ln (C/C_0) versus time of visible-light irradiation for TiO_2 and NC.

As a measurement of the effect that adding CDs to TiO_2 has on the photocatalytic efficiency, we calculated the extent of catalytic enhancement induced by the CDs addition using Eq. 3:

$$\%\ln(C) = \frac{k_{NC} - k_{TiO_2}}{k_{TiO_2}} \times 100 \quad (3)$$

Here, % ln (C) is a measure of the enhancement of TiO_2's catalytic efficiency upon adding CDs, k_{NC} is the reaction rate constant obtained with the catalytic NC, and k_{TiO2} is the reaction rate constant of TiO_2 under similar conditions.

The % ln(C) were calculated for all dyes, with a positive value, an indicator of an enhancement of the photocatalytic efficiency, being found only for MB (Table 2).

Table 2: Literature reports regarding the photodegradation of MB by different TiO_2-based NCs under visible-light irradiation.

Nanocomposite	CDs precursors	Pollutant	% ln (C)	Ref.
TiO_2 – CDs	CA + sawdust + EDA	MB	675	This work
TiO_2 – CDs	CA + Corn stover + EDA	MB	374	[152]
TiO_2 – CDs	CA + EDA	MB	367	[148]
Molecularly imprinted TiO_2 - CDs	Lignite + H_2O_2 + Formic acid	MB	64	[174]
TiO_2 – Ag - CDs	Ethylene glycol	MB	233	[175]
TiO_2 – Fe_2O_3 – CDs	CA + EDA	MB	366	[176]
Oxygen rich TiO_2 – Peroxo - CDs	CA + Urea	MB	130	[177]

The Table 2 show that, under visible-light irradiation, different TiO_2-based NCs exhibit distinct results on the MB photodegradation. It's possible to observe that the second NC achieved a very significant enhancement of the catalytic efficiency despite including corn stover as a co-carbon precursor. When compared to other works in the literature, most studies presented % ln(C) between 64% and 374%, which was way below the 675% enhancement obtained with the NC from this work, the one with sawdust as precursor.

For MB, the NC showed a remarkable 675% improvement in photodegradation compared to TiO_2, highlighting a significant performance enhancement associated with the incorporation of CDs. However, for the other dyes, the photocatalytic performance of the NC was lower than that of TiO_2, which is unexpected given the NC's superior intrinsic

properties, such as increased visible-light absorption, larger surface area, and reduced PL intensity. It is also important to note that, even in the cases where TiO_2 outperformed the NC, the %DR values remained relatively low. This is consistent with the well-known poor activity of TiO_2 under visible light, as expected from the band gap determined earlier. What stands out is that the NC, despite having improved intrinsic properties through the addition of CDs, did not exhibit better overall photocatalytic performance, suggesting that additional factors may be limiting its efficiency and that a deeper analysis is required to understand these results and the interplay between catalyst properties and responsiveness toward different dyes. These contrasting results suggest that additional factors influence the photocatalytic activity, warranting further investigation to better understand the interplay between catalyst properties and dye degradation behaviour.

Table 3: Photodegradation behaviours of each dye.

Dyes	**Composite**				**%In (C)**
	TiO_2		**NC**		
	%DR	**k (min^{-1})**	**%DR**	**k (min^{-1})**	
MB	6.80	0.0011	40.74	0.0087	674.75
MO	7.82	0.0013	5.84	0.0010	-20.56
RhB	17.43	0.0032	13.25	0.0023	-28.78
RBBR	32.90	0.0067	3.28	0.00058	-91.35
O. II	33.70	0.0066	10.69	0.0019	-71.67

In order to gain insights and understand why adding the CDs had different effects in the photocatalytic efficiency toward different organic dyes, we examined the effect of photolysis and adsorption, as well as the catalytic mechanism of the NC for three representative dyes that had different outcomes upon the addition of CDs: RhB, for which only a relatively moderate change was observed; MB, which exhibited enhanced photocatalytic efficiency; and Orange II, as that which resulted in a relevantly reduced performance by the NC. Via these experiments, we aim to explore how waste-derived photocatalytic NCs behave in the degradation of different organic dyes and better understand the mechanisms involved and the reasons behind the different outcomes depending on the pollutant.

Photolysis refers to the degradation of pollutants induced directly by light irradiation, without the involvement of a photocatalyst. To determine the contribution of photolysis to the %DR observed foreach of the three dyes, we measured the photodegradation in

the absence of the catalyst and compared it to the results obtained for TiO_2 and the NC. This step is important to verify whether the degradation observed is truly due to the photocatalytic activity of the materials, or if part of the effect originates from direct light-induced degradation, thus excluding external factors unrelated to the catalysts.

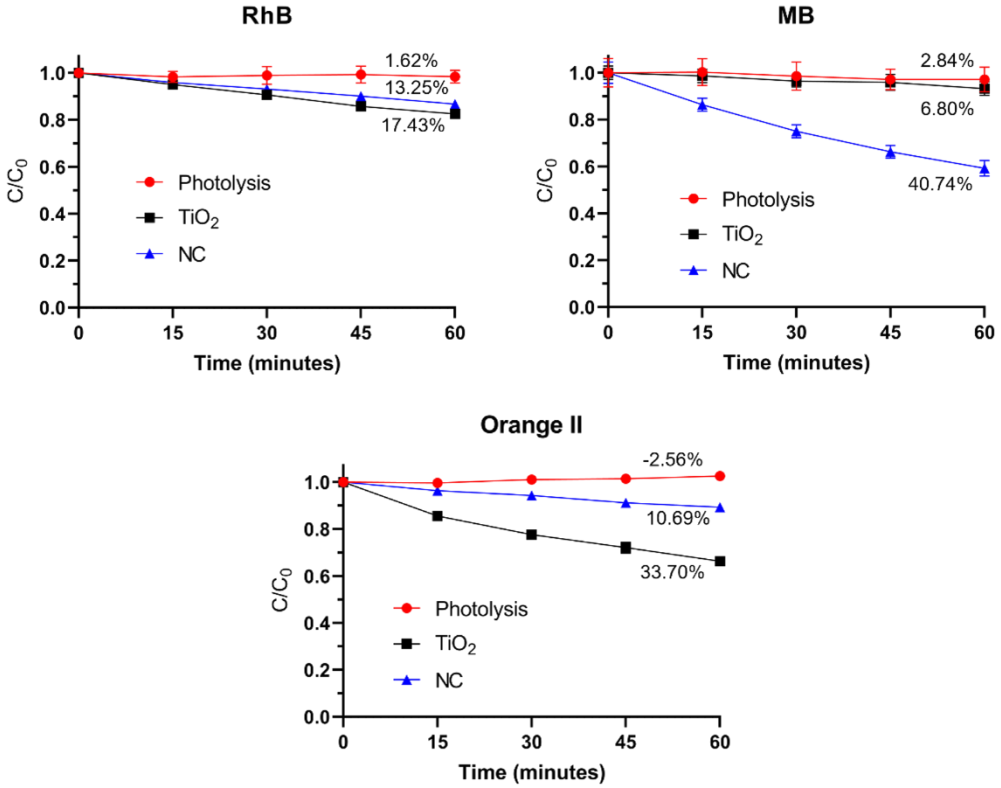

Figure 14: Effect of photolysis under visible light on the degradation of different dyes.

As we can see in Figure 14, the results indicate that no significant photolysis occurs within the time used for a typical photocatalytic assay. Photolysis alone is only responsible for a %DR of 1.62% for RhB, 2.84% for MB, and -2.56% for Orange II.

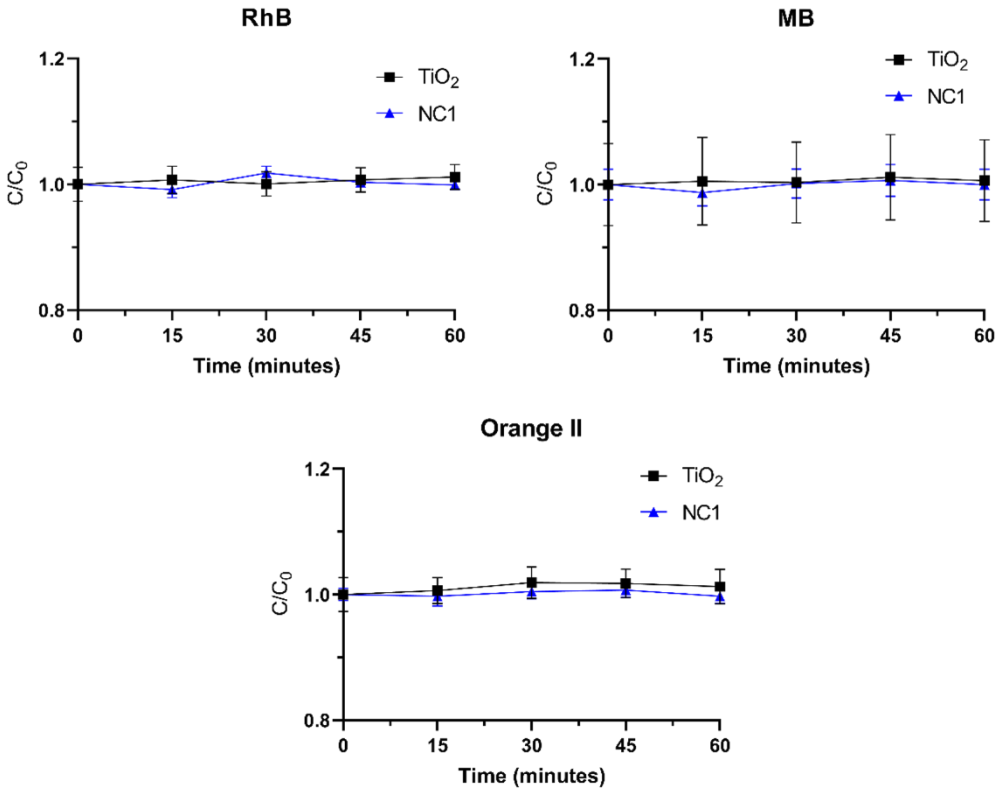

Figure 15: Adsorption of different dyes, in the absence of irradiation.

Furthermore, experiments in the absence of irradiation demonstrated that the effect of adsorption by the NC is virtually negligible. This step is essential to evaluate if the dye removal is due to a photocatalytic degradation or just the effect of adsorption of the dye by the pollutant, which does not necessarily mean that the pollutant is degraded. The results displayed in Figure 15 clearly demonstrate that the effect of adsorption is negligible. When conjugated, the results of the tests concerning photolysis and adsorption clearly demonstrate that the degradation observed in the photocatalytic assays is a direct result of the visible-light-driven activity of the photocatalysts rather than photolysis or adsorption by themselves.

3.3. Scavengers Test

One possible explanation for the differences in photocatalytic performance between TiO_2 and the NC may be related to their respective profiles of ROS generation. Scavenger assays using IPA and Tiron were conducted to gain insights regarding the reactive species partaking in the visible-light photodegradation of MB and better understand the catalytic mechanism of TiO_2 and the NC. These specific scavengers were selected because they target two of the most relevant ROS typically involved in TiO_2-based

photocatalysis: ●OH and $\bullet O_2^-$. The impact of each reactive species was assessed by quantifying the change in the %DR upon the addition of the tested scavengers. This change is calculated as follows (Eq. 4).

$$\%DRV = \%DR_{test} - \%DR_{control} \quad (4)$$

In this equation, %DRV corresponds to the %DR variation when a scavenger ($\%DR_{test}$) is added compared to a control test ($\%DR_{control}$, standard photodegradation with the catalyst).

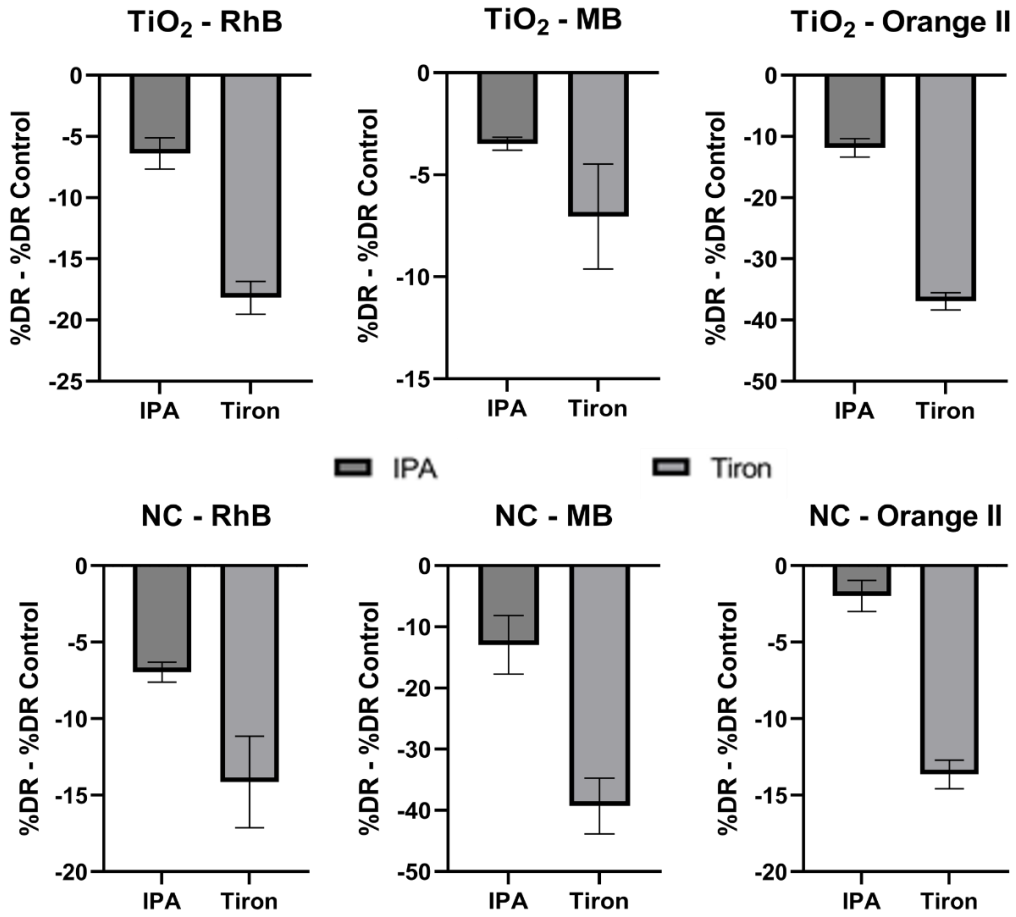

Figure 16: Visible-light-driven photodegradation of different dyes mediated by TiO_2 and NC, in the presence of reactive species scavengers (IPA (10 mM) > ●OH and Tiron (10 mM) > $\bullet O_2^-$). Results are presented as %DRV. A negative %DRV value indicates that the catalytic efficiency was hindered by the respective scavengers when compared to the control without scavengers.

As shown in Figure 16, the $\bullet O_2^-$ appears to be the main species behind the photocatalytic activity of the NC, while the ●OH plays a secondary role, as observed by the large decrease of the %DR in the presence of Tiron, followed by a smaller decrease in the presence of IPA (Table 4). Namely, for the NC, Tiron was led to a %DRV of -39.29%, -

14.14% and -13.64% for MB, RhB and Orange II, respectively. Whereas IPA led to decreases of -3.48%, -6.39% and -11.86%, respectively. It is worth noting that the results for Tiron show a %DRV in the scale of the %DR of the control, which is unexpected. One possible explanation for the large %DRV is that, although Tiron is commonly regarded as a selective scavenger for $\bullet O_2^-$, some literature reports indicate that it may also interact with ●OH. Thus, it may be scavenging both species in this system, which could account for the significant %DRV observed when compared to the control test [178].

Table 4: Scavengers impact on the degradation.

Composite	Dye	Scavenger	%DR	SD	%DRV
TiO_2	MB	None	6.81	0.32	N/A
		IPA	3.33	0.03	-3.48
		Tiron	-0.24	2.55	-7.05
	RhB	None	17.44	0.97	N/A
		IPA	11.06	0.84	-6.39
		Tiron	-0.74	0.92	-18.18
	Orange II	None	33.70	1.33	N/A
		IPA	21.84	0.67	-11.86
		Tiron	-3.24	0.48	-36.94
NC	MB	None	40.60	4.56	N/A
		IPA	27.66	1.43	-12.94
		Tiron	1.31	0.29	-39.29
	RhB	None	14.15	0.56	N/A
		IPA	7.19	0.33	-6.96
		Tiron	0.02	2.94	-14.14
	Orange II	None	10.69	0.85	N/A
		IPA	8.72	0.54	-1.98
		Tiron	-2.95	0.37	-13.64

Unravelling the reactive species behind the photocatalytic mechanism may provide insights regarding the different activities of the photocatalysts toward different organic dyes. Overall, the presence of scavengers for $\bullet O_2^-$ and ●OH led to a decrease in the observed %DR, indicating that both species contribute to the photodegradation mechanism, irrespective of the dye or the catalyst being TiO_2 or the NC. Their respective results suggests that they have similar scavenger profiles, with the photodegradation occurring primarily via $\bullet O_2^-$, with ●OH also playing a secondary but relevant role. Based on this, there is a chance that the NC may either produce a lower amount of radicals than TiO_2 or generate a mix of reactive species which favours the production of the less oxidative $\bullet O_2^-$ in detriment of the more oxidative ●OH. To explore this hypothesis, we monitored the degradation of SA and AA, two antioxidant probes that are known to

interact with ●OH and ●O_2^-, respectively, and thus can be used as a semi-quantitative method of measure the relative production of these ROS by TiO_2 and NC [179, 180].

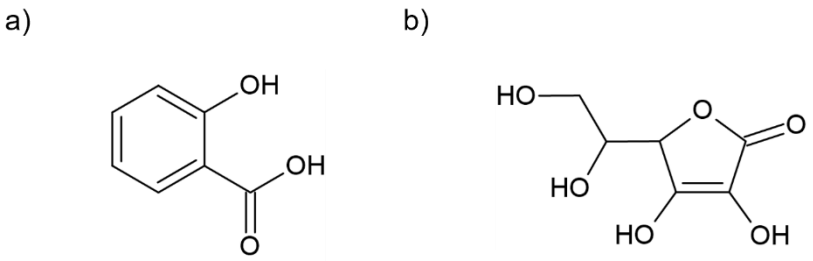

Figure 17: Molecular structure of a) SA and b) AA.

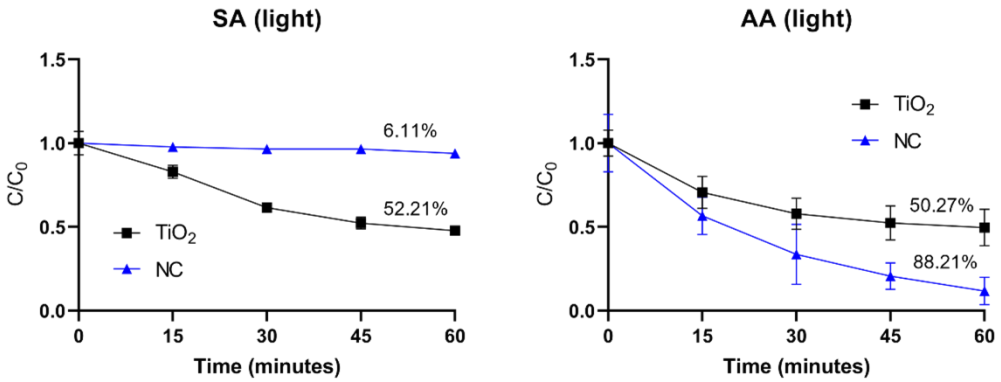

Figure 18: Visible-light-driven photodegradation mediated by TiO_2 and NC, in the presence of SA (10 mM) > ●OH and AA (10 mM) > ●O_2^-. Results are presented as variation of concentration of SA and AA.

As observed in Figure 18, under visible-light irradiation, TiO_2 causes a larger effect in SA than the NC. While TiO_2 degraded 52.21% of the initial SA concentration, with a degradation rate constant of 0.01300 min^{-1}, NC degraded 6.11% with a degradation rate constant of 0.00093 min^{-1}. This suggests that under the same conditions, TiO_2 may produce more ●OH than the NC, as this reactive specie is what is interacting with SA and degrading it. Regarding AA, the opposite was observed. That is, NC causes a higher degradation than TiO_2, with NC removing 88.21% of the initial AA and presenting a degradation rate constant of 0.035 min^{-1} while TiO_2 degraded 50.27% with a degradation rate constant of 0.011 min^{-1}. This suggests that the NC produces ●O_2^- on a larger scale than TiO_2, demonstrating that the two catalysts may have different rates of production for the different reactive species. Whereas the ●O_2^- may be the main reactive species

produced and contributor toward the photocatalytic activity of the NC, TiO_2 favours a relatively higher production of ●OH. Control experiments carried out in the dark indicated that no significant adsorption occurred during these assays. As a result of this, depending on the sensitivity of each dye toward the different reactive species, it may be more easily degraded by a specific reactive species, and thus a catalyst favouring the production of that species over the others is going to have an advantage in terms of photodegradation efficiency.

3.4. ORP tests

ORP tests were performed to evaluate the redox capacity of a system, indicating its tendency to promote oxidation or reduction reactions, as we want to test if NC produces more ●O_2^- than TiO_2. In photocatalytic processes, such as the degradation of organic dyes, ORP monitoring allows for the observation of reactive species generation over time and provides insight into the chemical environment of the solution. These measurements also enable the comparison of different catalytic materials, offering information on their relative efficiency in facilitating redox reactions. Moreover, ORP is widely used in environmental applications, such as water treatment, where it serves as an indicator of the chemical state of the system [181]. Therefore, ORP assays significantly contribute to the understanding of reaction mechanisms and to the optimization of photocatalytic material performance.

To better understand the results, we will do the treatment of the results using Eq. 5:

$$ORP = \frac{ORP_t}{ORP_0} \quad (5)$$

In this equation, ORP_t corresponds to the ORP values measured at different time points, while ORP_0 corresponds to the value recorded at t=0.

To perform these assays, 10 mg of TiO_2 or NC was added to a beaker containing 50 mL of deionised water. The suspension was first stirred in the dark for 30 minutes, followed by exposure to light under continuous stirring for another 30 minutes, during which any variations over time were recorded.

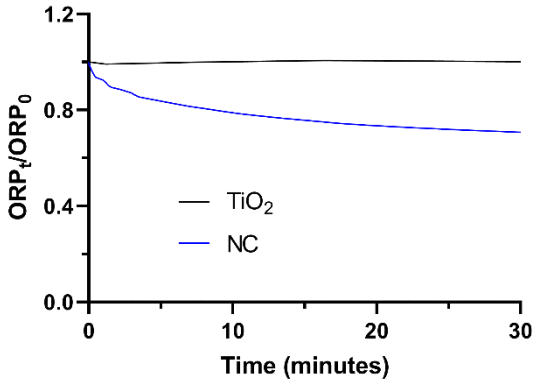

Figure 19: ORP tests for TiO_2 and NC.

In these experiments, we observed that, after the lamp is turned on, there is very little variation of the ORP for TiO_2 (Figure 19). This is expected, as it is well known that TiO_2 has poor visible-light activity. On the other hand, the NC shows a significant change upon turning on the lamp, which is consistent with its enhanced visible-light activity. Namely, a marked decrease in the ORP values was observed for the NC, which indicates that it is generating a more reducing rather than oxidizing environment upon irradiation, contrary to what one might expect. Furthermore, during the ORP experiment for NC, after approximately 30 minutes, the ORP seems to stabilize.

TiO_2 and TiO_2-based photocatalysts (such as the NC) are known to create an oxidative environment upon light irradiation, as they generate ROS, such as ●OH and $●O_2^-$, which are responsible for degrading pollutants in water through oxidation [182]. However, this oxidative activity only occurs when pollutants are present in the system to react with the ROS. In our experiment, only TiO_2 or the NC are suspended in water, meaning the only measurable reactions via ORP are those related to ROS generation, which are primarily ●OH and $●O_2^-$. As is well known, ●OH are formed through the oxidation of water by the photocatalyst, whereas $●O_2^-$ result from the reduction of dissolved oxygen. If the former reaction predominates, the ORP profile will likely reflect increased oxidation (ORP increase). If both reactions occur in a balanced manner, the profile will remain more neutral. Conversely, if the latter reaction predominates, the ORP will exhibit a more reductive trend (ORP decrease).

In our case, we observed the latter for the NC a significant decrease in ORP values upon light exposure, indicating a more reductive environment, which aligns with the predominant formation of $●O_2^-$ that was already observed in the test with AA [183]. The ORP profile of TiO_2, on the other hand, showed a very slight decrease followed by a slight increase, which is consistent with a more balanced generation of $●O_2^-$ (reduction)

and ●OH (oxidation), as observed in the tests with AA and SA, caused a %DR of ~50% for both compounds. Therefore, the results support our hypothesis that NC produces more $\bullet O_2^-$ than TiO_2. Since $\bullet O_2^-$ is less oxidative than ●OH, this explains why the NC does not always outperform TiO_2 under visible light, despite exhibiting a higher photonic efficiency, higher visible-light absorption, and a larger surface area (as determined by BET analysis).

3.5. Mechanism Interpretation

Based on the results obtained, we hypothesize that, while in the photocatalytic mechanism a larger absorption of visible light and better photonic efficiency prompts a larger production and better maintenance of photogenerated charge carriers, it may do so in an uneven manner. Namely, NC appears to favour the production of $\bullet O_2^-$ rather than ●OH while TiO_2 appears to be relatively equilibrated regarding the reactive species it produces. The increased formation of $\bullet O_2^-$ is not unique to this NC but has also been observed in other TiO_2-based photocatalysts modified with CDs. In fact, CDs are known to possess abundant surface states and oxygen-containing functional groups [87, 184], facilitating charge separation [185] and promoting the reduction of molecular oxygen to superoxide [186, 187]. Considering this, the dominance of superoxide-driven photodegradation aligns well with previous studies concerning TiO_2/CDs NCs using CDs [175, 176]. The enhanced formation of superoxide is consistent with the superior degradation observed for MB, while other dyes such as MO, RhB, Orange II and RBBR exhibit lower degradation efficiencies. These findings suggest that the incorporation of CDs into TiO_2, by shifting the resulting ROS profile toward $\bullet O_2^-$ formation, may have different outcomes toward different organic dyes depending on their sensitivity to each specific reactive species. Namely, while MB may be more sensitive to the $\bullet O_2^-$ favoured by the NC, the other dyes may not be as sensitive and thus the increased superoxide output in detriment of the ●OH may not be beneficial for the photodegradation of those dyes that may require more oxidizing species. This mechanistic understanding is critical for the rational design of photocatalysts tailored to specific pollutant types.

4. Conclusions and Future Works

4.1. Conclusions

This work aimed to investigate how photocatalytic NC performed in the photodegradation of different organic dyes by understanding the underlying mechanisms and the reasons behind the variation in efficiency among the contaminants. By testing the catalysts for the degradation of different dyes under visible light, the work aimed to identify differences in degradation efficiency. UV-Vis and PL spectroscopy, photolysis, SEM, FTIR and BET analysis as well as species scavenging and ORP measurements were used to characterize the materials and investigate the reactive species involved and the redox behaviour of the system, respectively

In a first stage, we successfully synthesized NCs using waste-derived materials for the photodegradation of organic pollutants. The resulting NC exhibited enhanced photocatalytic efficiency toward MB, presenting a 675% improvement of the catalytic efficiency. However, the incorporation of CDs showed no improvement, or even a detrimental effect on the degradation performance of other dyes. This suggests that different pollutants may respond distinctly to the mixture of reactive species generated by the catalyst.

The results from the tests with reactive species scavengers indicate that $\bullet O_2^-$ are the primary reactive species responsible for the photocatalytic activity of the NC, while $^{\cdot}OH$ play a secondary role. Further studies with AA and SA revealed that TiO_2 and the NC produced $\bullet OH$ and $\bullet O_2^{\cdot-}$ at different rates, with the NC favouring the production of the $O_2^{\cdot-}$ while TiO_2 originates similar amounts of $^{\cdot}OH$ and $O_2^{\cdot-}$, which was further confirmed by the results from the ORP test. Considering that each dye has a specific sensitivity to the different ROS, this could explain why the incorporation of CDs does not consistently enhance the photocatalytic performance of the NC across different organic dyes. As a result, the presence of CDs may lead to varying effects depending on the dye in question by promoting the formation of one reactive species over the other.

Due to this, further studies are necessary to determine the origin of the differences in catalytic efficiency observed with the different dyes.

The key conclusion drawn from this study is that, depending on the target pollutant, it is essential to understand how different degradation pathways are influenced, and to tailor the system according to the mechanisms that can optimize its performance.

4.2. Future Works

In the future, it would be valuable to further explore the development of clean, zero-waste technologies for the removal of highly persistent pollutants from water sources, using only sunlight as the energy input, as it is a clean and inexhaustible energy source that could be used for power the treatment of wastewater.

To build upon the findings of this study, several follow-up investigations and experiments could be pursued:

This present work uses a fixed irradiation time, 1 hour, for all photocatalytic tests. While this approach enabled meaningful comparisons between catalysts, future experiments should extend the irradiation period until maximum dye degradation is achieved, allowing the determination of the final degradation efficiencies and a better kinetic modeling.

It would also be valuable to analyze the degradation by-products formed during the photocatalytic process. Identifying and quantifying intermediate compounds through other techniques may provide insights into the degradation mechanisms and the environmental safety of the process.

Another promising direction is the optimization of the NC formulation. While sawdust-derived CDs were used in this work, other waste sources could potentially yield CDs with improved optoelectronic properties or surface functionality. Exploring alternative biomass precursors, such as corn stover, or doping strategies may enhance the activity of the composite catalyst.

Finally, long-term stability and recyclability tests of the NC should be conducted under realistic conditions to assess its viability for practical applications. Investigating the photocatalytic performance under natural sunlight and in real wastewater matrices would further support the potential for environmental implementation and the scalability of the process.

References

1. Cuerda-Correa, E.M., M.F. Alexandre-Franco, and C. Fernández-González, *Advanced Oxidation Processes for the Removal of Antibiotics from Water. An Overview.* Water, 2019. **12**(1).
2. Oturan, M.A. and J.-J. Aaron, *Advanced Oxidation Processes in Water/Wastewater Treatment: Principles and Applications. A Review.* Critical Reviews in Environmental Science and Technology, 2014. **44**(23): p. 2577-2641.
3. Mekonnen, M.M. and A.Y. Hoekstra, *Four billion people facing severe water scarcity.* Sci Adv, 2016. **2**(2): p. e1500323.
4. Niemczynowicz, J., *Urban hydrology and water management – present and future challenges.* Urban Water, 1999. **1**(1): p. 1-14.
5. Ma, X., et al., *Sustainable Water Systems for the City of Tomorrow—A Conceptual Framework.* Sustainability, 2015. **7**(9): p. 12071-12105.
6. Pal, A., et al., *Emerging contaminants of public health significance as water quality indicator compounds in the urban water cycle.* Environ Int, 2014. **71**: p. 46-62.
7. Kumar, R., et al., *A review on emerging water contaminants and the application of sustainable removal technologies.* Case Studies in Chemical and Environmental Engineering, 2022. **6**.
8. Wilson, H.M., et al., *Biomass-derived porous carbon for excellent low intensity solar steam generation and seawater desalination.* Solar Energy Materials and Solar Cells, 2020. **215**.
9. Ruan, T., et al., *Identification and Prioritization of Environmental Organic Pollutants: From an Analytical and Toxicological Perspective.* Chem Rev, 2023. **123**(17): p. 10584-10640.
10. Guo, Z., et al., *Stabilized Mo2S3 by FeS2 based porous solar evaporation systems for highly efficient clean freshwater collection.* Solar Energy Materials and Solar Cells, 2020. **211**.
11. Chen, Z., et al., *Recent progress on sorption/desorption-based atmospheric water harvesting powered by solar energy.* Solar Energy Materials and Solar Cells, 2021. **230**.
12. Salehi, A.A., et al., *A review on the water-energy nexus for drinking water production from humid air.* Renewable and Sustainable Energy Reviews, 2020. **120**.

13. Lundqvist, J., et al., *Innovative drinking water treatment techniques reduce the disinfection-induced oxidative stress and genotoxic activity.* Water Res, 2019. **155**: p. 182-192.
14. Srithar, K. and T. Rajaseenivasan, *Recent fresh water augmentation techniques in solar still and HDH desalination – A review.* Renewable and Sustainable Energy Reviews, 2018. **82**: p. 629-644.
15. Ruhi, A., et al., *Bioaccumulation and trophic magnification of pharmaceuticals and endocrine disruptors in a Mediterranean river food web.* Sci Total Environ, 2016. **540**: p. 250-9.
16. Huerta, B., et al., *Development of an extraction and purification method for the determination of multi-class pharmaceuticals and endocrine disruptors in freshwater invertebrates.* Talanta, 2015. **132**: p. 373-81.
17. Rodriguez-Narvaez, O.M., et al., *Treatment technologies for emerging contaminants in water: A review.* Chemical Engineering Journal, 2017. **323**: p. 361-380.
18. Annamalai, J. and V. Namasivayam, *Endocrine disrupting chemicals in the atmosphere: Their effects on humans and wildlife.* Environ Int, 2015. **76**: p. 78-97.
19. Bhatia, D., et al., *Biological methods for textile dye removal from wastewater: A review.* Critical Reviews in Environmental Science and Technology, 2017. **47**(19): p. 1836-1876.
20. Gaur, N., K. Narasimhulu, and P. Y, *Recent advances in the bio-remediation of persistent organic pollutants and its effect on environment.* Journal of Cleaner Production, 2018. **198**: p. 1602-1631.
21. Wang, L. and M.F. Modest, *Narrow-Band Based Multiscale Full-Spectrum k-Distribution Method for Radiative Transfer in Inhomogeneous Gas Mixtures.* Journal of Heat Transfer, 2005. **127**(7): p. 740-748.
22. Trojanowicz, M., *Removal of persistent organic pollutants (POPs) from waters and wastewaters by the use of ionizing radiation.* Sci Total Environ, 2020. **718**: p. 134425.
23. Kelly, B.C., et al., *Food web-specific biomagnification of persistent organic pollutants.* Science, 2007. **317**(5835): p. 236-9.
24. Venkatesan, A.K. and R.U. Halden, *Wastewater treatment plants as chemical observatories to forecast ecological and human health risks of manmade chemicals.* Sci Rep, 2014. **4**: p. 3731.

25. Chawla, H., S.K. Singh, and A.K. Haritash, *Reversing the damage: ecological restoration of polluted water bodies affected by pollutants due to anthropogenic activities.* Environ Sci Pollut Res Int, 2024. **31**(1): p. 127-143.
26. Siddiqua, A., J.N. Hahladakis, and W. Al-Attiya, *An overview of the environmental pollution and health effects associated with waste landfilling and open dumping.* Environ Sci Pollut Res Int, 2022. **29**(39): p. 58514-58536.
27. Wolff, M.S., *Endocrine disruptors: challenges for environmental research in the 21st century.* Ann N Y Acad Sci, 2006. **1076**: p. 228-38.
28. Ali, I., et al., *Thalidomide: A Banned Drug Resurged into Future Anticancer Drug.* Current Drug Therapy, 2012. **7**(1): p. 13-23.
29. Goldstein, S., *Beta-blocking drugs and coronary heart disease.* Cardiovasc Drugs Ther, 1997. **11 Suppl 1**: p. 219-25.
30. Chaput, J.P., E. Doucet, and A. Tremblay, *Obesity: a disease or a biological adaptation? An update.* Obes Rev, 2012. **13**(8): p. 681-91.
31. Guo, Y.L., et al., *Yucheng: health effects of prenatal exposure to polychlorinated biphenyls and dibenzofurans.* Int Arch Occup Environ Health, 2004. **77**(3): p. 153-8.
32. De Tata, V., *Association of dioxin and other persistent organic pollutants (POPs) with diabetes: epidemiological evidence and new mechanisms of beta cell dysfunction.* Int J Mol Sci, 2014. **15**(5): p. 7787-811.
33. Vizcaino, E., et al., *Transport of persistent organic pollutants across the human placenta.* Environ Int, 2014. **65**: p. 107-15.
34. Hanafi, M.F. and N. Sapawe, *A review on the current techniques and technologies of organic pollutants removal from water/wastewater.* Materials Today: Proceedings, 2020. **31**: p. A158-A165.
35. Saravanan, A., et al., *Effective water/wastewater treatment methodologies for toxic pollutants removal: Processes and applications towards sustainable development.* Chemosphere, 2021. **280**: p. 130595.
36. Kumari, P. and A. Kumar, *ADVANCED OXIDATION PROCESS: A remediation technique for organic and non-biodegradable pollutant.* Results in Surfaces and Interfaces, 2023. **11**.
37. Perelo, L.W., *Review: In situ and bioremediation of organic pollutants in aquatic sediments.* J Hazard Mater, 2010. **177**(1-3): p. 81-9.
38. Gaur, N., et al., *Recent advances in the elimination of persistent organic pollutants by photocatalysis.* Frontiers in Environmental Science, 2022. **10**.

39. Van Thuan, D., et al., *Photodegradation of hazardous organic pollutants using titanium oxides -based photocatalytic: A review.* Environ Res, 2023. **229**: p. 116000.
40. Zhang, N., et al., *Ag NPs decorated on the magnetic Fe3O4@PDA as efficient catalyst for organic pollutants removal and as effective antimicrobial agent for microbial inhibition.* Journal of Alloys and Compounds, 2022. **928**.
41. Malato, S., et al., *Decontamination and disinfection of water by solar photocatalysis: Recent overview and trends.* Catalysis Today, 2009. **147**(1): p. 1-59.
42. Zhang, F., et al., *Recent Advances and Applications of Semiconductor Photocatalytic Technology.* Applied Sciences, 2019. **9**(12).
43. Spasiano, D., et al., *Solar photocatalysis: Materials, reactors, some commercial, and pre-industrialized applications. A comprehensive approach.* Applied Catalysis B: Environmental, 2015. **170-171**: p. 90-123.
44. Sendao, R.M.S., J.C.G. Esteves da Silva, and L. Pinto da Silva, *Photocatalytic removal of pharmaceutical water pollutants by TiO(2) - Carbon dots nanocomposites: A review.* Chemosphere, 2022. **301**: p. 134731.
45. Wang, J. and S. Wang, *Effect of inorganic anions on the performance of advanced oxidation processes for degradation of organic contaminants.* Chemical Engineering Journal, 2021. **411**.
46. Hubner, U., et al., *Advanced oxidation processes for water and wastewater treatment - Guidance for systematic future research.* Heliyon, 2024. **10**(9): p. e30402.
47. Zhang, D.E., et al., *Synthesis and photocatalytic property of multilayered Co 3 O 4.* Applied Surface Science, 2015. **355**: p. 547-552.
48. Iervolino, G., et al., *Limitations and Prospects for Wastewater Treatment by UV and Visible-Light-Active Heterogeneous Photocatalysis: A Critical Review.* Top Curr Chem (Cham), 2019. **378**(1): p. 7.
49. Linsebigler, A.L., G. Lu, and J.T. Yates, *Photocatalysis on TiO2 Surfaces: Principles, Mechanisms, and Selected Results.* Chemical Reviews, 2002. **95**(3): p. 735-758.
50. Fujishima, A. and K. Honda, *Electrochemical photolysis of water at a semiconductor electrode.* Nature, 1972. **238**(5358): p. 37-8.
51. Chen, X. and S.S. Mao, *Titanium dioxide nanomaterials: synthesis, properties, modifications, and applications.* Chem Rev, 2007. **107**(7): p. 2891-959.

52. Ren, G., et al., *Recent Advances of Photocatalytic Application in Water Treatment: A Review.* Nanomaterials (Basel), 2021. **11**(7).
53. Ahmari, H., S.Z. Heris, and M.H. Khayyat, *The effect of titanium dioxide nanoparticles and UV irradiation on photocatalytic degradation of Imidaclopride.* Environ Technol, 2018. **39**(4): p. 536-547.
54. Loeb, S.K., et al., *The Technology Horizon for Photocatalytic Water Treatment: Sunrise or Sunset?* Environ Sci Technol, 2019. **53**(6): p. 2937-2947.
55. Kabra, K., R. Chaudhary, and R.L. Sawhney, *Treatment of Hazardous Organic and Inorganic Compounds through Aqueous-Phase Photocatalysis: A Review.* Industrial & Engineering Chemistry Research, 2004. **43**(24): p. 7683-7696.
56. Ibrahim, M.M., et al., *Direct Z-scheme of Cu2O/TiO2 enhanced self-cleaning, antibacterial activity, and UV protection of cotton fiber under sunlight.* Applied Surface Science, 2019. **479**: p. 953-962.
57. Poursani, A.S., et al., *The Synthesis of Nano TiO₂ and Its Use for Removal of Lead Ions from Aqueous Solution.* Journal of Water Resource and Protection, 2016. **08**(04): p. 438-448.
58. Gong, M., et al., *Research progress of photocatalytic sterilization over semiconductors.* RSC Adv, 2019. **9**(34): p. 19278-19284.
59. Perovic, K., et al., *Recent Achievements in Development of TiO(2)-Based Composite Photocatalytic Materials for Solar Driven Water Purification and Water Splitting.* Materials (Basel), 2020. **13**(6).
60. Anitha, B. and M.A. Khadar, *Anatase-rutile phase transformation and photocatalysis in peroxide gel route prepared TiO2 nanocrystals: Role of defect states.* Solid State Sciences, 2020. **108**.
61. Tanji, K., et al., *Fast photodegradation of rhodamine B and caffeine using ZnO-hydroxyapatite composites under UV-light illumination.* Catalysis Today, 2022. **388-389**: p. 176-186.
62. Suhan, M.B.K., et al., *Sustainable pollutant removal and wastewater remediation using TiO2-based nanocomposites: A critical review.* Nano-Structures & Nano-Objects, 2023. **36**.
63. Zhang, X., et al., *Preparation and photocatalytic wettability conversion of TiO2-based superhydrophobic surfaces.* Langmuir, 2006. **22**(23): p. 9477-9.
64. Seo, M.K. and S.J. Park, *Surface characteristics of carbon fibers modified by direct oxyfluorination.* J Colloid Interface Sci, 2009. **330**(1): p. 237-42.
65. Zheng, Z., et al., *Strategic synthesis of hierarchical TiO2 microspheres with enhanced photocatalytic activity.* Chemistry, 2010. **16**(37): p. 11266-70.

66. Nagaraj, K., et al., *Photocatalytic advancements and applications of titanium dioxide (TiO_2): Progress in biomedical, environmental, and energy sustainability.* Next Research, 2025. **2**(1).
67. Rengifo-Herrera, J.A. and C. Pulgarin, *Why five decades of massive research on heterogeneous photocatalysis, especially on TiO2, has not yet driven to water disinfection and detoxification applications? Critical review of drawbacks and challenges.* Chemical Engineering Journal, 2023. **477**.
68. Ren, W., et al., *Low temperature preparation and visible light photocatalytic activity of mesoporous carbon-doped crystalline TiO2.* Applied Catalysis B: Environmental, 2007. **69**(3-4): p. 138-144.
69. Daghrir, R., P. Drogui, and D. Robert, *Photoelectrocatalytic technologies for environmental applications.* Journal of Photochemistry and Photobiology A: Chemistry, 2012. **238**: p. 41-52.
70. Dong, H., et al., *An overview on limitations of TiO2-based particles for photocatalytic degradation of organic pollutants and the corresponding countermeasures.* Water Res, 2015. **79**: p. 128-46.
71. Gao, B., et al., *Adsorption-photocatalytic degradation of Acid Red 88 by supported TiO2: Effect of activated carbon support and aqueous anions.* Chemical Engineering Journal, 2011. **171**(3): p. 1098-1107.
72. Zhou, M., et al., *Pt nanocrystallines/TiO2 with thickness-controlled carbon layers: Preparation and activities in CO oxidation.* Chinese Chemical Letters, 2018. **29**(6): p. 787-790.
73. Nur, A.S.M., et al., *A review on the development of elemental and codoped TiO2 photocatalysts for enhanced dye degradation under UV–vis irradiation.* Journal of Water Process Engineering, 2022. **47**.
74. Liu, H., et al., *Organic cocatalysts improved Fenton and Fenton-like processes for water pollution control: A review.* Chemosphere, 2024. **353**: p. 141581.
75. Zhang, Y., et al., *Magnetron-sputtering fabrication of noble metal nanodots coated TiO 2 nanoparticles with enhanced photocatalytic performance.* Materials & Design, 2017. **125**: p. 94-99.
76. Kovalchuk, A., et al., *Luminescent Polymer Composite Films Containing Coal-Derived Graphene Quantum Dots.* ACS Appl Mater Interfaces, 2015. **7**(47): p. 26063-8.
77. Yang, W., et al., *Carbon nanomaterials in biosensors: should you use nanotubes or graphene?* Angew Chem Int Ed Engl, 2010. **49**(12): p. 2114-38.

78. De Jong, K.P. and J.W. Geus, *Carbon Nanofibers: Catalytic Synthesis and Applications.* Catalysis Reviews, 2007. **42**(4): p. 481-510.
79. Ozyurt, D., et al., *Properties, synthesis, and applications of carbon dots: A review.* Carbon Trends, 2023. **12**.
80. Fernandes, S., J.C.G. Esteves da Silva, and L. Pinto da Silva, *Comparative life cycle assessment of high-yield synthesis routes for carbon dots.* NanoImpact, 2021. **23**: p. 100332.
81. Fernandes, S., J.C.G. Esteves da Silva, and L. Pinto da Silva, *Life Cycle Assessment-Based Comparative Study between High-Yield and "Standard" Bottom-Up Procedures for the Fabrication of Carbon Dots.* Materials (Basel), 2022. **15**(10).
82. Xu, X., et al., *Electrophoretic analysis and purification of fluorescent single-walled carbon nanotube fragments.* J Am Chem Soc, 2004. **126**(40): p. 12736-7.
83. Sun, Y.P., et al., *Quantum-sized carbon dots for bright and colorful photoluminescence.* J Am Chem Soc, 2006. **128**(24): p. 7756-7.
84. Alas, M.O., et al., *Fluorescent carbon dots are the new quantum dots: an overview of their potential in emerging technologies and nanosafety.* Journal of Materials Science, 2020. **55**(31): p. 15074-15105.
85. Zhu, S., et al., *Highly photoluminescent carbon dots for multicolor patterning, sensors, and bioimaging.* Angew Chem Int Ed Engl, 2013. **52**(14): p. 3953-7.
86. Baker, S.N. and G.A. Baker, *Luminescent carbon nanodots: emergent nanolights.* Angew Chem Int Ed Engl, 2010. **49**(38): p. 6726-44.
87. Esteves da Silva, J.C.G. and H.M.R. Gonçalves, *Analytical and bioanalytical applications of carbon dots.* TrAC Trends in Analytical Chemistry, 2011. **30**(8): p. 1327-1336.
88. Lim, S.Y., W. Shen, and Z. Gao, *Carbon quantum dots and their applications.* Chem Soc Rev, 2015. **44**(1): p. 362-81.
89. Crista, D.M.A., J.C.G. Esteves da Silva, and L. Pinto da Silva, *Evaluation of Different Bottom-up Routes for the Fabrication of Carbon Dots.* Nanomaterials (Basel), 2020. **10**(7).
90. Jiang, M., et al., *Multicolor luminescence of carbon Dots: From mechanisms to applications.* Chemical Engineering Journal, 2024. **496**.
91. Jie, L., et al., *A review of CdS photocatalytic nanomaterials: Morphology, synthesis methods, and applications.* Materials Science in Semiconductor Processing, 2024. **176**.

92. Kaczmarek, A., et al., *Luminescent Carbon Dots Synthesized by the Laser Ablation of Graphite in Polyethylenimine and Ethylenediamine.* Materials (Basel), 2021. **14**(4).
93. Li, N., et al., *Synthesis of semiconducting SWNTs by arc discharge and their enhancement of water splitting performance with TiO2 photocatalyst.* Carbon, 2011. **49**(15): p. 5132-5141.
94. Calabro, R.L., D.S. Yang, and D.Y. Kim, *Liquid-phase laser ablation synthesis of graphene quantum dots from carbon nano-onions: Comparison with chemical oxidation.* J Colloid Interface Sci, 2018. **527**: p. 132-140.
95. Han, Z., et al., *Hydrothermal synthesis of carbon dots and their application for detection of chlorogenic acid.* Luminescence, 2020. **35**(7): p. 989-997.
96. Singh, R.K., et al., *Progress in microwave-assisted synthesis of quantum dots (graphene/carbon/semiconducting) for bioapplications: a review.* Materials Today Chemistry, 2019. **12**: p. 282-314.
97. Li, X., et al., *Carbonized wood loaded with carbon dots for preparation long-term shape-stabilized composite phase change materials with superior thermal energy conversion capacity.* Renewable Energy, 2021. **174**: p. 19-30.
98. Huang, H., et al., *A one-step ultrasonic irradiation assisted strategy for the preparation of polymer-functionalized carbon quantum dots and their biological imaging.* J Colloid Interface Sci, 2018. **532**: p. 767-773.
99. Bressi, V., et al., *Recent advances in the synthesis of carbon dots from renewable biomass by high-efficient hydrothermal and microwave green approaches.* Current Opinion in Green and Sustainable Chemistry, 2023. **40**.
100. Chan, H.K. and P.C. Kwok, *Production methods for nanodrug particles using the bottom-up approach.* Adv Drug Deliv Rev, 2011. **63**(6): p. 406-16.
101. Yang, Z.C., et al., *Intrinsically fluorescent carbon dots with tunable emission derived from hydrothermal treatment of glucose in the presence of monopotassium phosphate.* Chem Commun (Camb), 2011. **47**(42): p. 11615-7.
102. Zhu, H., et al., *Microwave synthesis of fluorescent carbon nanoparticles with electrochemiluminescence properties.* Chem Commun (Camb), 2009(34): p. 5118-20.
103. Wang, L. and H.S. Zhou, *Green synthesis of luminescent nitrogen-doped carbon dots from milk and its imaging application.* Anal Chem, 2014. **86**(18): p. 8902-5.

104. Jiang, K., et al., *Red, green, and blue luminescence by carbon dots: full-color emission tuning and multicolor cellular imaging.* Angew Chem Int Ed Engl, 2015. **54**(18): p. 5360-3.
105. Pan, D., et al., *Hydrothermal route for cutting graphene sheets into blue-luminescent graphene quantum dots.* Adv Mater, 2010. **22**(6): p. 734-8.
106. Wang, R., et al., *Recent progress in carbon quantum dots: synthesis, properties and applications in photocatalysis.* Journal of Materials Chemistry A, 2017. **5**(8): p. 3717-3734.
107. Xiong, Y., et al., *Influence of molecular fluorophores on the research field of chemically synthesized carbon dots.* Nano Today, 2018. **23**: p. 124-139.
108. Peng, Z., et al., *Carbon dots: Biomacromolecule interaction, bioimaging and nanomedicine.* Coordination Chemistry Reviews, 2017. **343**: p. 256-277.
109. Vale, N., et al., *Normal breast epithelial MCF-10A cells to evaluate the safety of carbon dots.* RSC Med Chem, 2021. **12**(2): p. 245-253.
110. Wang, K., et al., *Systematic safety evaluation on photoluminescent carbon dots.* Nanoscale Res Lett, 2013. **8**(1): p. 122.
111. Sendão, R.M.S., et al., *Insight into the hybrid luminescence showed by carbon dots and molecular fluorophores in solution.* Phys Chem Chem Phys, 2019. **21**(37): p. 20919-20926.
112. Hola, K., et al., *Graphitic Nitrogen Triggers Red Fluorescence in Carbon Dots.* ACS Nano, 2017. **11**(12): p. 12402-12410.
113. Tian, M., et al., *Yellow-emitting carbon dots for selective detecting 4-NP in aqueous media and living biological imaging.* Spectrochim Acta A Mol Biomol Spectrosc, 2019. **220**: p. 117117.
114. Belkahla, H., et al., *Carbon dots, a powerful non-toxic support for bioimaging by fluorescence nanoscopy and eradication of bacteria by photothermia.* Nanoscale Adv, 2019. **1**(7): p. 2571-2579.
115. Afonso, A.C.P., et al., *An Active Surface Preservation Strategy for the Rational Development of Carbon Dots as pH-Responsive Fluorescent Nanosensors.* Chemosensors, 2021. **9**(8).
116. Simoes, E.F.C., et al., *Hypochlorite fluorescence sensing by phenylboronic acid-alizarin adduct based carbon dots.* Talanta, 2020. **208**: p. 120447.
117. Crista, D.M.A., et al., *3-Hydroxyphenylboronic Acid-Based Carbon Dot Sensors for Fructose Sensing.* J Fluoresc, 2019. **29**(1): p. 265-270.

118. Hettiarachchi, S.D., et al., *Triple conjugated carbon dots as a nano-drug delivery model for glioblastoma brain tumors.* Nanoscale, 2019. **11**(13): p. 6192-6205.
119. He, H., et al., *Diketopyrrolopyrrole-based carbon dots for photodynamic therapy.* Nanoscale, 2018. **10**(23): p. 10991-10998.
120. Joseph, J. and A.A. Anappara, *White-Light-Emitting Carbon Dots Prepared by the Electrochemical Exfoliation of Graphite.* Chemphyschem, 2017. **18**(3): p. 292-298.
121. Kalytchuk, S., et al., *Carbon Dot Nanothermometry: Intracellular Photoluminescence Lifetime Thermal Sensing.* ACS Nano, 2017. **11**(2): p. 1432-1442.
122. Zhang, Y.-Q., et al., *N-doped carbon quantum dots for TiO2-based photocatalysts and dye-sensitized solar cells.* Nano Energy, 2013. **2**(5): p. 545-552.
123. Lee, D.-E., et al., *State-of-the-art review on photocatalysis for efficient wastewater treatment: Attractive approach in photocatalyst design and parameters affecting the photocatalytic degradation.* Catalysis Communications, 2023. **183**.
124. Zhu, D. and Q. Zhou, *Action and mechanism of semiconductor photocatalysis on degradation of organic pollutants in water treatment: A review.* Environmental Nanotechnology, Monitoring & Management, 2019. **12**.
125. Sabri, M., A. Habibi-Yangjeh, and S. Vadivel, *Activation of persulfate ions by TiO2/carbon dots nanocomposite under visible light for photocatalytic degradations of organic contaminants.* Journal of Materials Science: Materials in Electronics, 2019. **30**(13): p. 12510-12522.
126. Li, H., et al., *Water-soluble fluorescent carbon quantum dots and photocatalyst design.* Angew Chem Int Ed Engl, 2010. **49**(26): p. 4430-4.
127. Rahbar, M., et al., *S, N co-doped carbon quantum dots/TiO(2) nanocomposite as highly efficient visible light photocatalyst.* Nanotechnology, 2019. **30**(50): p. 505702.
128. Chen, P., et al., *Study on the photocatalytic mechanism and detoxicity of gemfibrozil by a sunlight-driven TiO2/carbon dots photocatalyst: The significant roles of reactive oxygen species.* Applied Catalysis B: Environmental, 2017. **204**: p. 250-259.
129. Lin, X., et al., *Carbon dots based on natural resources: Synthesis and applications in sensors.* Microchemical Journal, 2021. **160**.

130. Bridgwater, T., *Biomass for energy.* Journal of the Science of Food and Agriculture, 2006. **86**(12): p. 1755-1768.
131. Neves, S.A. and A.C. Marques, *Drivers and barriers in the transition from a linear economy to a circular economy.* Journal of Cleaner Production, 2022. **341**.
132. Wang, F., et al., *Technologies and perspectives for achieving carbon neutrality.* The Innovation, 2021. **2**(4).
133. Adegoke, K.A., et al., *Sawdust-biomass based materials for sequestration of organic and inorganic pollutants and potential for engineering applications.* Current Research in Green and Sustainable Chemistry, 2022. **5**.
134. Xiang, J., et al., *Performance study of high energy storage supercapacitor from waste corn husk biomass electrode materials.* Journal of Physics and Chemistry of Solids, 2024. **194**.
135. Dias, J.M., et al., *Waste materials for activated carbon preparation and its use in aqueous-phase treatment: a review.* J Environ Manage, 2007. **85**(4): p. 833-46.
136. Algarra, M., et al., *Sustainable Production of Carbon Nanoparticles from Olive Pit Biomass: Understanding Proton Transfer in the Excited State on Carbon Dots.* ACS Sustainable Chemistry & Engineering, 2019. **7**(12): p. 10493-10500.
137. Brandao, A., et al., *Renewable Carbon Materials as Electrodes for High-Performance Supercapacitors: From Marine Biowaste to High Specific Surface Area Porous Biocarbons.* ACS Omega, 2023. **8**(21): p. 18782-18798.
138. Brandao, A., et al., *Chitins from Seafood Waste as Sustainable Porous Carbon Precursors for the Development of Eco-Friendly Supercapacitors.* Materials (Basel), 2023. **16**(6).
139. Brandão, A.T.S.C., et al., *Porous Carbon Materials Based on Blue Shark Waste for Application in High-Performance Energy Storage Devices.* Applied Sciences, 2023. **13**(15).
140. Omokafe, S.M., et al., *Fabrication of Activated Carbon from Coconut Shells and its Electrochemical Properties for Supercapacitors.* International Journal of Electrochemical Science, 2020. **15**(11): p. 10854-10865.
141. Pourhosseini, S.E.M., et al., *Synthesis of a Novel Interconnected 3D Pore Network Algal Biochar Constituting Iron Nanoparticles Derived from a Harmful Marine Biomass as High-Performance Asymmetric Supercapacitor Electrodes.* ACS Sustainable Chemistry & Engineering, 2018. **6**(4): p. 4746-4758.

142. Crista, D.M.A., J.C.G.E. da Silva, and L.P. da Silva, *Validation of Spent Coffee Grounds as Precursors for the Development of Sustainable Carbon Dot-Based for Fe3+ Optical Sensing.* Chemistry Proceedings, 2021. **5**(1): p. 17.
143. Crista, D.M.A., et al., *Turning Spent Coffee Grounds into Sustainable Precursors for the Fabrication of Carbon Dots.* Nanomaterials (Basel), 2020. **10**(6).
144. Mohan, D., et al., *Organic and inorganic contaminants removal from water with biochar, a renewable, low cost and sustainable adsorbent--a critical review.* Bioresour Technol, 2014. **160**: p. 191-202.
145. Fernandes, S., et al., *Development of a Facile and Green Synthesis Strategy for Brightly Fluorescent Carbon Dots from Various Waste Materials.* ChemSusChem, 2025. **18**(2): p. e202401702.
146. Li, H., et al., *Recent advances in carbon dots for bioimaging applications.* Nanoscale Horizons, 2020. **5**(2): p. 218-234.
147. Qiao, G., et al., *Rapid conversion from common precursors to carbon dots in large scale: Spectral controls, optical sensing, cellular imaging and LEDs application.* J Colloid Interface Sci, 2020. **580**: p. 88-98.
148. Sendão, R.M.S., et al., *Carbon Dots–TiO2Nanocomposites for the Enhanced Visible-Light Driven Photodegradation of Methylene Blue.* Advanced Sustainable Systems, 2023. **8**(1).
149. Sendao, R.M.S., J.C.G. Esteves da Silva, and L. Pinto da Silva, *Comparative life cycle assessment of the fabrication of visible-light-driven photocatalytic TiO(2) - Carbon dots nanocomposites for wastewater treatment.* NanoImpact, 2025. **38**: p. 100556.
150. Zhang, J., et al., *N-doped carbon quantum dots/TiO2 hybrid composites with enhanced visible light driven photocatalytic activity toward dye wastewater degradation and mechanism insight.* Journal of Photochemistry and Photobiology A: Chemistry, 2016. **325**: p. 104-110.
151. Zhang, J., et al., *Visible-light-driven pollutants degradation with carbon quantum dots/N-TiO2 under mild condition: Facile preparation, dramatic performance and deep mechanism insight.* Colloids and Surfaces A: Physicochemical and Engineering Aspects, 2020. **601**.
152. Sendão, R.M.S., et al., *Visible-light-driven photocatalytic degradation of organic dyes using a TiO2 and waste-based carbon dots nanocomposite.* Colloids and Surfaces A: Physicochemical and Engineering Aspects, 2025. **713**.

153. El Mragui, A., et al., *Synthesis of Fe- and Co-Doped TiO(2) with Improved Photocatalytic Activity Under Visible Irradiation Toward Carbamazepine Degradation.* Materials (Basel), 2019. **12**(23).
154. El Mragui, A., O. Zegaoui, and J.C.G. Esteves da Silva, *Elucidation of the photocatalytic degradation mechanism of an azo dye under visible light in the presence of cobalt doped TiO(2) nanomaterials.* Chemosphere, 2021. **266**: p. 128931.
155. Melgoza, D., A. Hernandez-Ramirez, and J.M. Peralta-Hernandez, *Comparative efficiencies of the decolourisation of Methylene Blue using Fenton's and photo-Fenton's reactions.* Photochem Photobiol Sci, 2009. **8**(5): p. 596-9.
156. Rodríguez, E.M., et al., *Determination of main species involved in the first steps of TiO2 photocatalytic degradation of organics with the use of scavengers: The case of ofloxacin.* Applied Catalysis B: Environmental, 2015. **178**: p. 44-53.
157. Zuo, F., et al., *Self-doped Ti3+ enhanced photocatalyst for hydrogen production under visible light.* J Am Chem Soc, 2010. **132**(34): p. 11856-7.
158. Tong, S., et al., *Preparation of carbon quantum dots/TiO2 composite and application for enhanced photodegradation of rhodamine B.* Colloids and Surfaces A: Physicochemical and Engineering Aspects, 2022. **648**.
159. Tang, S., et al., *Enhanced photocatalytic H2 production performance of CdS hollow spheres using C and Pt as bi-cocatalysts.* Chinese Journal of Catalysis, 2021. **42**(5): p. 743-752.
160. Guo, Z., et al., *Phosphorus-doped graphene quantum dots loaded on TiO2 for enhanced photodegradation.* Applied Surface Science, 2020. **526**.
161. Hatefi, R., et al., *A facile decoration of anatase Fe3O4/TiO2 nanocomposite with graphene quantum dots: Synthesis, characterization, and photocatalytic activity.* Advanced Powder Technology, 2021. **32**(7): p. 2410-2422.
162. Ru, Y., G.I.N. Waterhouse, and S. Lu, *Aggregation in carbon dots.* Aggregate, 2022. **3**(6).
163. Barrett, E.P., L.G. Joyner, and P.P. Halenda, *The Determination of Pore Volume and Area Distributions in Porous Substances. I. Computations from Nitrogen Isotherms.* Journal of the American Chemical Society, 2002. **73**(1): p. 373-380.
164. Feizpoor, S., A. Habibi-Yangjeh, and K. Yubuta, *Integration of carbon dots and polyaniline with TiO2 nanoparticles: Substantially enhanced photocatalytic activity to removal various pollutants under visible light.* Journal of Photochemistry and Photobiology A: Chemistry, 2018. **367**: p. 94-104.

165. Fang, Y., et al., *Co-modified Commercial P25 TiO2 by Fe Doping and g-C3N4 Coating as High Performance Photocatalyst under visible light irradiation.* International Journal of Electrochemical Science, 2017. **12**(7): p. 5951-5963.
166. Cardoso, I.M.F., et al., *UV-Based Advanced Oxidation Processes of Remazol Brilliant Blue R Dye Catalyzed by Carbon Dots.* Nanomaterials (Basel), 2022. **12**(12).
167. Rajender, G., J. Kumar, and P.K. Giri, *Interfacial charge transfer in oxygen deficient TiO2-graphene quantum dot hybrid and its influence on the enhanced visible light photocatalysis.* Applied Catalysis B: Environmental, 2018. **224**: p. 960-972.
168. Li, Y., et al., *Kinetic study and model of the photocatalytic degradation of rhodamine B (RhB) by a TiO2-coated activated carbon catalyst: Effects of initial RhB content, light intensity and TiO2 content in the catalyst.* Chemical Engineering Journal, 2008. **142**(2): p. 147-155.
169. Haji, S., B. Benstaali, and N. Al-Bastaki, *Degradation of methyl orange by UV/H2O2 advanced oxidation process.* Chemical Engineering Journal, 2011. **168**(1): p. 134-139.
170. Li, G., et al., *Electrochemically assisted photocatalytic degradation of Orange II: Influence of initial pH values.* Journal of Molecular Catalysis A: Chemical, 2006. **259**(1-2): p. 238-244.
171. Liu, Y., J. Huang, and X. Zhang, *Decolorization and biodegradation of remazol brilliant blue R by bilirubin oxidase.* J Biosci Bioeng, 2009. **108**(6): p. 496-500.
172. Patil, S.S., A. Sukhdev, and S. Chandrasekaran, *Visible light-driven efficient photocatalytic degradation of organic dyes by conducting polymer/Fe and Cu doped ZnO photocatalyst.* Optical Materials, 2025. **165**.
173. Saquib, M. and M. Muneer, *Semiconductor mediated photocatalysed degradation of an anthraquinone dye, Remazol Brilliant Blue R under sunlight and artificial light source.* Dyes and Pigments, 2002. **53**(3): p. 237-249.
174. Yu, J., et al., *Facile synthesis of molecularly imprinted black TiO2-x/carbon dots nanocomposite and its recognizable photocatalytic performance under visible-light.* Applied Surface Science, 2021. **551**.
175. Wang, C., et al., *One-pot solvothermal synthesis of carbon dots/Ag nanoparticles/TiO2 nanocomposites with enhanced photocatalytic performance.* Ceramics International, 2018. **44**(18): p. 22481-22488.

176. Zhang, J., et al., *Fabrication of carbon quantum dots/TiO2/Fe2O3 composites and enhancement of photocatalytic activity under visible light.* Chemical Physics Letters, 2019. **730**: p. 391-398.
177. Feizpoor, S., et al., *Oxygen-rich TiO2 decorated with C-Dots: Highly efficient visible-light-responsive photocatalysts in degradations of different contaminants.* Advanced Powder Technology, 2019. **30**(6): p. 1183-1196.
178. Weng, C., et al., *Targeted Antibacterial Strategy Based on Reactive Oxygen Species Generated from Dioxygen Reduction Using an Organoruthenium Complex.* JACS Au, 2021. **1**(9): p. 1348-1354.
179. Peralta, E., et al., *Hydroxyl Radicals quantification by UV spectrophotometry.* Electrochimica Acta, 2014. **129**: p. 137-141.
180. Nandi, A. and I.B. Chatterjee, *Scavenging of superoxide radical by ascorbic acid.* Journal of Biosciences, 1987. **11**(1-4): p. 435-441.
181. Chen, K.C., et al., *Real-time control of an immobilized-cell reactor for wastewater treatment using ORP.* Water Res, 2002. **36**(1): p. 230-8.
182. Kohantorabi, M., G. Moussavi, and S. Giannakis, *A review of the innovations in metal- and carbon-based catalysts explored for heterogeneous peroxymonosulfate (PMS) activation, with focus on radical vs. non-radical degradation pathways of organic contaminants.* Chemical Engineering Journal, 2021. **411**.
183. Fustier, P., et al., *Non-enzymatic browning and ascorbic acid degradation of orange juice subjected to electroreduction and electro-oxidation treatments.* Innovative Food Science & Emerging Technologies, 2011. **12**(4): p. 491-498.
184. Hola, K., et al., *Carbon dots—Emerging light emitters for bioimaging, cancer therapy and optoelectronics.* Nano Today, 2014. **9**(5): p. 590-603.
185. Zhao, Q., et al., *Built-in electric field-assisted charge separation over carbon dots-modified Bi2WO6 nanoplates for photodegradation.* Applied Surface Science, 2019. **465**: p. 164-171.
186. Tyagi, A., et al., *Green synthesis of carbon quantum dots from lemon peel waste: applications in sensing and photocatalysis.* RSC Advances, 2016. **6**(76): p. 72423-72432.
187. Cui, L., et al., *Carbon Dots: Synthesis, Properties and Applications.* Nanomaterials (Basel), 2021. **11**(12).